J. Fluid Mech. (2004), *vol.* 510, *pp.* 267–302.
DOI: 10.1017/S0022112004009516 Printed in the United Kingdom

Three-dimensional Green's function for harmonic water waves over a bottom topography with different depths at infinity

By K. A. BELIBASSAKIS AND G. A. ATHANASSOULIS

School of Naval Architecture and Marine Engineering, Section of Ship and Marine Hydrodynamics, National Technical University of Athens

kbel@fluid.mech,ntua.gr; mathan@central.ntua.gr

(Received 8 August 2003 and in revised form 4 February 2004)

The three-dimensional Green's function of water waves in variable-bathymetry regions, associated with the problem of propagation of water waves emitted from a monochromatic point source, is derived and studied. The solution is of interest in its own right but also provides useful information for the formulation and treatment of complex wave–body–seabed interaction problems in variable-bathymetry regions, especially as regards the hydrodynamic characteristics of large structures installed in the nearshore and coastal environment. Assuming a parallel-contour bathymetry, with a continuous depth function of the form $h(x, y) = h(x)$, attaining constant, but possibly different, values at the semi-infinite regions $x < a$ and $x > b$, the problem is reduced to a two-dimensional one, by using Fourier transform. The transformed problem is treated by applying domain decomposition and reformulating it as a transmission problem in the finite domain containing the bottom irregularity. An appropriate decomposition of the wave potential is introduced, permitting the singular part to be solved analytically, and the problem for the regular part to be reformulated as a variational problem. An enhanced local-mode series representation is used for the regular wave potential in the variable-bathymetry region, including the propagating mode, the sloping-bottom mode (see Athanassoulis & Belibassakis 1999), and a number of evanescent modes. Using this representation, in conjunction with the variational principle, a forced system of horizontal coupled-mode equations is derived for the determination of the complex modal-amplitude functions of the regular wave potential. This system is numerically solved by using a second-order central finite-difference scheme. The source-generated water-wave potential is, finally, obtained by an efficient numerical Fourier inversion based on FFT. Numerical results are presented and discussed for various bottom topographies, including smooth but steep underwater trenches and ridges, putting emphasis on the identification of the important features of the near- and far-field patterns on the horizontal plane and on the vertical plane containing the point source. Characteristic patterns of trapped (well-localized) wave propagation over ridges are predicted and discussed.

1. Introduction

Water-wave interaction with floating and/or immersed bodies, in variable-bathymetry regions with different depths at infinity, is an interesting and mathematically difficult problem, especially when all characteristic lengths are of the same order of magnitude, and no assumptions concerning mildness of bottom slope are introduced.

This class of problems is further complicated by the fact that the physical properties of the medium (the depth and thus the propagation speed) are different at infinity as approached from different directions. In this case, the far-field wave pattern is not known *a priori*, and thus its asymptotic form at infinity is part of the problem.

The present work deals with the construction and the efficient numerical calculation of the three-dimensional Green's function for harmonic water waves over an uneven bottom topography. This Green's function permits one to formulate and solve three-dimensional wave–body interaction problems in variable-bathymetry regions with different depths at infinity, by means of boundary integral equations supported only on the wetted surface of the scatterers (bodies). The solution of these problems is of great practical importance for many applications, for example the hydrodynamic analysis of large floating structures (megafloats) in the nearshore and coastal environment. Although the nonlinearity of water waves is also of great importance, it seems unavoidable to start by studying the linearized version of the problem. One of our main concerns in formulating and studying this problem is to investigate the far-field wave pattern which, in this case, is expected to be azimuthally strongly anisotropic.

Similar problems of harmonic-wave interaction with localized scatterers or inclusions in non-uniform media, characterized by a variable index of refraction, are also frequently encountered in applications related to acoustic, elastic and electromagnetic wave propagation. Felsen & Marcuvitz (1973) and Brekhovskikh & Godin (1992) present an excellent account of solutions of acoustic and electromagnetic radiation and scattering problems in continuously stratified and layered media.

The first derivation of the Green's function of harmonic water waves in the case of a water layer of constant depth was given by John (1950); see also Wehausen & Laitone (1960, § 13) and Mei (1986, Ch. 7). Thorne (1953) studied the whole sequence of singular solutions (source, dipole, multipoles) for infinite depth and constant finite depth. The latter case was further studied by Newman (1985) with emphasis on developing efficient algorithms for numerical calculations. John's solution has been generalized by Evans (1972) to the case of two half-strips of constant but different depths, with application to the problem of oblique transmission of water waves over a shelf of arbitrary profile. The Green's function of the mild-slope equation, for the case of a mildly sloped bottom topography connecting two areas of different depths, has been studied by Belibassakis (2000), putting emphasis on the investigation of the structure of the far field. It is shown that, in the case of a monotonic bed profile, the main characteristics of the far field are: (i) the formation of a shadow zone with an ever expanding width, which is located above the bottom shoaling, and (ii) in each of the two sectors not including the area of variable depth, the asymptotic behaviour of the wave field approaches the form of an outgoing cylindrical wave, propagating with an amplitude of $O(\rho^{-1/2})$, where ρ is the horizontal distance from the source, and wavelength corresponding to the sector depth at infinity. On the other hand, in the shadow zone, a weak wave system is outgoing at infinity with amplitude of $O(\rho^{-3/2})$, consisting of the superposition of two waves with wavelengths corresponding to the two depths at infinity (Belibassakis 2000, § 3). In the case of non-monotonic bed profiles as, for example, in the case of a source over a smooth underwater ridge, duct propagation at specific frequencies could occur, corresponding to the appearance of guided modes (or trapped waves) over the ridge; see e.g. Mei (1983, Ch. 4.6).

In the present work, the three-dimensional Green's function of harmonic water waves in a parallel-contour bathymetry connecting two shelves of constant, yet different, depth is derived and studied. This work generalizes the results of Belibassakis (2000) to the general bathymetry case, without any assumption concerning the vertical

structure of the wave field like, for example, the one imposed by the mild-slope approximation.

The structure of this paper is as follows. In § 2 the differential formulation of the problem is presented, both in physical and in Fourier-transformed space, under the assumption that all physical length scales, i.e. the wavelengths, the bottom variation length and the depths, are considered comparable. Thus, no asymptotic assumptions are introduced for them, and no restrictions are imposed concerning the magnitude of bottom slope and/or curvature. Since the bottom geometry is assumed to be invariant with respect to one horizontal direction, the problem is treated by means of a Fourier transform. By applying domain decomposition, the Fourier-transformed problem is reformulated as a two-dimensional transmission problem in the finite interval containing the variable-depth bottom. Specific care is taken in extending the formulation in the complex Fourier domain, enabling, at a subsequent step, a robust numerical inversion by means of FFT.

In § 3, a decomposition of the Green's function to an analytically invertible singular part and a regular part is made, permitting the efficient treatment of the singularity in physical space. In § 4, a variational principle is presented for the regular part of the wave potential, which, in conjunction with an enhanced local-mode series expansion, leads to a coupled-mode system of equations for the determination of the complex modal amplitudes. The enhanced local-mode series expansion, which was first introduced and studied by Athanassoulis & Belibassakis (1999), contains as well as the usual propagating and evanescent modes, an additional term, called the sloping-bottom mode, enabling the consistent satisfaction of the boundary condition on the non-horizontal parts of the bottom. The rate of convergence of the enhanced local-mode series is fast (of $O(n^{-4})$), and thus only a few terms are required to obtain accurate results. In § 5, the numerical scheme for solving the coupled-mode system and implementing the fast Fourier inversion is presented and tested in simple cases, where the exact solution is analytically known. In § 6 numerical results are presented and discussed for various bottom topographies, including smooth but steep underwater shoals, trenches and ridges, aimed at the identification of the important features of the near- and far-field patterns on the horizontal and the vertical planes. Finally, in § 7, the application of the present Green's function to three-dimensional wave–body–seabed interaction problems in variable-bathymetry regions is discussed. Two Appendices contain results concerning the case of a point source lying far from the bottom irregularity, and the leading-order far-field asymptotics of the source field.

2. Differential formulation of the problem

The marine environment studied consists of a horizontally unbounded water layer D_{3D}, confined between a free surface $\partial D_{F,3D}$ and a rigid bottom $\partial D_{\Pi,3D}$. It is assumed that the bathymetry exhibits an arbitrary one-dimensional variation, and thus it is characterized by parallel, straight bottom contours lying between two regions of constant but possibly different depth, $h = h_1$ and $h = h_3$. Without loss of generality we assume $h_3 \leqslant h_1$; see figure 1. The liquid is assumed homogeneous, inviscid and incompressible, and the flow is excited by a pulsating monochromatic point source of angular frequency ω, located in D_{3D}.

A Cartesian coordinate system is introduced, with its origin at some point on the mean water level, the z-axis pointing upwards and the y-axis parallel to the bottom contours; see figure 1. The liquid domain D_{3D} will be represented by $D_{3D} = D \times R$, where D is the (two-dimensional) intersection of D_{3D} by a vertical plane perpendicular

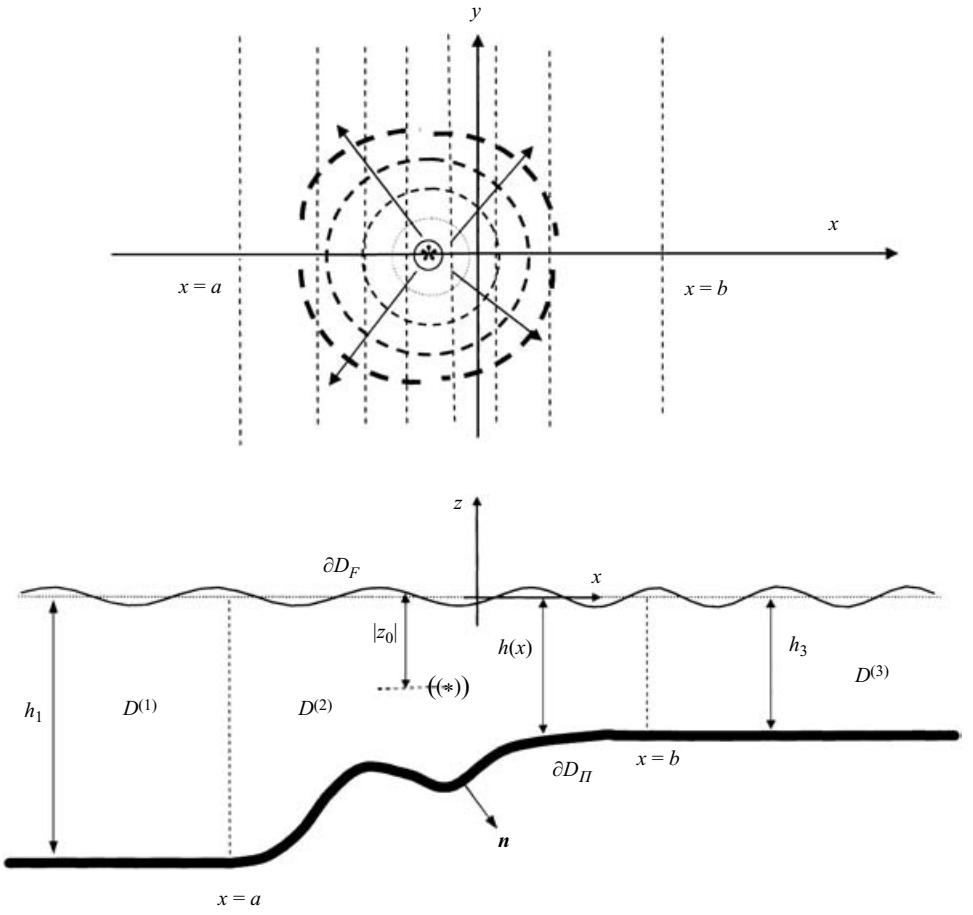

FIGURE 1. Domain decomposition and basic notation. The point source is denoted by an asterisk.

to the bottom contours, and $R = (-\infty, +\infty)$. The local depth, measured from the mean water level, is described by a smooth, y-independent function $h(x, y) = h(x)$, which is considered to be twice continuously differentiable. In accordance with this description

$$h(x) = h(a) = h_1 \quad \text{for all} \quad x \leqslant a, \quad h(x) = h(b) = h_3 \quad \text{for all} \quad x \geqslant b. \tag{2.1}$$

The liquid domain is decomposed in three subdomains $D_{3D}^{(m)} = D^{(m)} \times R$, $m = 1, 2, 3$, defined as follows: $D_{3D}^{(1)}$ is the constant-depth subdomain characterized by $x < a$, $D_{3D}^{(3)}$ is the constant-depth subdomain characterized by $x > b$, and $D_{3D}^{(2)}$ is the variable bathymetry subdomain lying between $D_{3D}^{(1)}$ and $D_{3D}^{(3)}$. Similar decompositions are applied to the free-surface and bottom boundaries. Finally, we define the vertical interfaces $\partial D_I^{(12)}$ and $\partial D_I^{(23)}$ separating the three subdomains, which are vertical segments (between the bottom and the mean water level) at $x = a$ and $x = b$, respectively. See figure 1.

2.1. *The boundary value problem*

In the context of linearized water-wave theory, see e.g. Stoker (1957) or Wehausen & Laitone (1960), the time-harmonic wave potential corresponding to a pulsating source

located at $\boldsymbol{r}_0 = (x_0, y_0, z_0)$ is given by

$$\tilde{\Phi}(\boldsymbol{r}, \boldsymbol{r}_0; t) = \mathrm{Re}\{\Phi(\boldsymbol{r}, \boldsymbol{r}_0; \mu)\exp(-\mathrm{i}\omega t)\}, \tag{2.2}$$

where $\boldsymbol{r} = (x, y, z)$, $\mathrm{i} = \sqrt{-1}$, $\mu = \omega^2/g$ is the frequency parameter, g is the acceleration due to gravity, and $\Phi(\boldsymbol{r}, \boldsymbol{r}_0; \mu)$ satisfies the problem

$$\frac{\partial^2\Phi}{\partial x^2} + \frac{\partial^2\Phi}{\partial y^2} + \frac{\partial^2\Phi}{\partial z^2} = -\delta(\boldsymbol{r} - \boldsymbol{r}_0), \quad \boldsymbol{r} \in D_{3D}, \tag{2.3a}$$

$$\frac{\partial\Phi}{\partial z} - \mu\Phi = 0, \quad \boldsymbol{r} \in \partial D_{F,3D}, \quad \frac{\partial\Phi}{\partial n} = 0, \quad \boldsymbol{r} \in \partial D_{\Pi,3D}. \tag{2.3b,c}$$

Φ along with its spatial derivatives is bounded and behaves like outgoing waves as

$$\rho = \sqrt{(x - x_0)^2 + (y - y_0)^2} \to \infty. \tag{2.3d}$$

Without loss of generality we assume that $y_0 = 0$. The boundary value problem (2.3) will be referred to as the three-dimensional *wave problem* $\mathscr{P}_{3D}(D_{3D}, \mu, \boldsymbol{r}_0)$. Since the geometry of the domain and the forcing of this problem are symmetric with respect to y, it is expected that the solution $\Phi(\boldsymbol{r}, \boldsymbol{r}_0; \mu)$ exhibits the same symmetry.

The present development will focus on the case where the point source is located inside the variable-bathymetry region, i.e. $\boldsymbol{x}_0 = (x_0, z_0) \in D^{(2)}$. This seems to be the most interesting case from the point of view of applications (e.g. wave–body interaction problems) in the nearshore and coastal environment, usually characterized by depth variations. Also, if the source lies in one of the two constant-depth subregions $D^{(1)}$ or $D^{(3)}$, close to the ends of the variable-depth subdomain $D^{(2)}$ (at a distance of a few wavelengths), the present approach is directly applicable by artificially extending the subdomain $D^{(2)}$ to include the point source. The other case, where the point source lies in $D^{(m)}$, $m = 1$ or 3, at a great distance from $D^{(2)}$, is simpler and it is discussed in Appendix A.

Exploiting the cylindrical character of the geometry of the liquid domain in the horizontal sense, i.e. $D_{3D} = D \times R$, it is possible to reduce the dimensionality of the problem by one, by taking the Fourier transform with respect to y. The transformed wave potential will be denoted by $\varphi(\boldsymbol{x}, \boldsymbol{x}_0; \xi)$, where $\boldsymbol{x} = (x, z)$ and $\boldsymbol{x}_0 = (x_0, z_0)$. The following pair of equations clarifies our conventions regarding the 2π-factors and exponent signs in the Fourier transform:

$$\varphi(\boldsymbol{x}, \boldsymbol{x}_0; \xi) = \frac{1}{2\pi}\int_{-\infty}^{+\infty} \Phi(\boldsymbol{r}, \boldsymbol{r}_0; \mu)\mathrm{e}^{-\mathrm{i}y\xi}\,\mathrm{d}y, \quad \Phi(\boldsymbol{r}, \boldsymbol{r}_0, \mu) = \int_{-\infty}^{+\infty} \varphi(\boldsymbol{x}, \boldsymbol{x}_0; \xi)\mathrm{e}^{+\mathrm{i}y\xi}\,\mathrm{d}\xi. \tag{2.4a,b}$$

Applying the Fourier transform to the problem $\mathscr{P}_{3D}(D_{3D}, \mu, \boldsymbol{r}_0)$, we obtain the following family of two-dimensional wave problems ($\xi \in R$):

$$\nabla^2\varphi - \xi^2\varphi = -\frac{1}{2\pi}\delta(x - x_0)\delta(z - z_0) \quad \text{in} \quad D, \tag{2.5a}$$

$$\frac{\partial\varphi}{\partial z} - \mu\varphi = 0 \quad \text{on} \quad \partial D_F, \quad \frac{\partial\varphi}{\partial n} = 0 \quad \text{on} \quad \partial D_\Pi, \tag{2.5b,c}$$

φ along with its spatial derivatives is bounded and

$$\text{behaves like outgoing waves as } |x| \to \infty, \tag{2.5d}$$

where $\nabla^2 \equiv \partial^2/\partial x^2 + \partial^2/\partial z^2$ denotes the two-dimensional Laplacian on the vertical plane. The family of boundary value problems (2.5) is referred to as the *transformed wave problem* $\mathscr{P}_\xi(D, \mu, \boldsymbol{x}_0)$. The source point being fixed, the transformed wave

potential $\varphi(\boldsymbol{x}, \boldsymbol{x}_0; \xi)$ will sometimes denoted by $\varphi(x, z; \xi)$. Since the solution of the three-dimensional problem is y-symmetric, the transformed wave potential $\varphi(\boldsymbol{x}, \boldsymbol{x}_0; \xi)$ will also be symmetric with respect to the real Fourier parameter ξ. Thus, it is possible to consider the problem $\mathscr{P}_\xi(D, \mu, \boldsymbol{x}_0)$ only for $\xi \in R^+$, and then extend the solution to $\xi \in R^-$ by symmetry, i.e.

$$\varphi(\boldsymbol{x}, \boldsymbol{x}_0; \xi) = \varphi(\boldsymbol{x}, \boldsymbol{x}_0; -\xi), \quad \xi \in R^-. \tag{2.6}$$

2.2. *The matching-boundary value problem in the variable depth subdomain*

For any value of the Fourier parameter $\xi \in R^+$ (except, possibly a discrete subset of values corresponding to the singularities of $\varphi(x, z; \xi)$ lying on the positive real axis; see below), the transformed wave problem can be reformulated as a transmission problem in the finite subdomain $D^{(2)}$. To this end, the following, general representations of the potential $\varphi(x, z; \xi)$ in the semi-infinite strips $D^{(1)}$ and $D^{(3)}$, obtained by separation of variables (see e.g. Evans 1972; Miles 1967), will be used:

Left half-strip $D^{(1)}$ $(x \leqslant a)$:

$$\varphi^{(1)}(x, z; \xi) = C_0^{(1)}(\xi) \exp\big(-\mathrm{i}x, \mathscr{K}_0^{(1)}(\xi)\big) Z_0^{(1)}(z) + \sum_{n=1}^{\infty} C_n^{(1)}(\xi) Z_n^{(1)}(z) \exp\big((x-a)\mathscr{K}_n^{(1)}(\xi)\big), \tag{2.7a}$$

Right half-strip $D^{(3)}$ $(x \geqslant b)$:

$$\varphi^{(3)}(x, z; \xi) = C_0^{(3)}(\xi) \exp\big(\mathrm{i}x, \mathscr{K}_0^{(3)}(\xi)\big) Z_0^{(3)}(z) + \sum_{n=1}^{\infty} C_n^{(3)}(\xi) Z_n^{(3)}(z) \exp\big(-(x-b)\mathscr{K}_n^{(3)}(\xi)\big), \tag{2.7b}$$

where

$$\mathscr{K}_0^{(m)}(\xi) = \sqrt{\big(k_0^{(m)}\big)^2 - \xi^2}, \quad \mathscr{K}_n^{(m)}(\xi) = \sqrt{\big(k_n^{(m)}\big)^2 + \xi^2}, \quad n = 1, 2, \ldots, \quad m = 1, 3. \tag{2.8}$$

The coefficients $C_n^{(m)}(\xi) \equiv C_n^{(m)}$, $m = 1, 3$, $n = 0, 1, 2, \ldots$, apearing in (2.7), will be determined by means of the appropriate matching conditions at the interfaces $\partial D_I^{(12)}$ and $\partial D_I^{(23)}$. The sets of numbers $\{\mathrm{i}k_0^{(m)}, k_n^{(m)}, n = 1, 2, \ldots\}$, and the sets of vertical functions $\{Z_n^{(m)}(z), n = 0, 1, 2, \ldots\}, m = 1, 3$, appearing in (2.7) and (2.8), are, respectively, the eigenvalues and the corresponding eigenfunctions of the following regular Sturm–Liouville problems:

$$\frac{\mathrm{d}^2 Z^{(m)}(z)}{\mathrm{d}z^2} + \big(k_n^{(m)}\big)^2 Z^{(m)}(z) = 0, \quad -h_m < z < 0, \tag{2.9a}$$

$$\frac{\mathrm{d}Z^{(m)}(0)}{\mathrm{d}z} - \mu Z^{(m)}(0) = 0, \quad \frac{\mathrm{d}Z^{(m)}(-h_m)}{\mathrm{d}z} = 0, \tag{2.9b,c}$$

which are obtained, respectively, by separation of variables in the half-strips $D^{(m)}, m = 1, 3$. The eigenvalues $\{\mathrm{i}k_0^{(m)}, k_n^{(m)}\}, m = 1, 3$, are obtained as the roots of the dispersion relations

$$\mu h_m = -k^{(m)} h_m \tan\big(k^{(m)} h_m\big), \quad m = 1, 3, \tag{2.10a}$$

and the eigenfunctions $\{Z_n^{(m)}(z), n=0, 1, 2, \ldots\}$ are given by

$$Z_0^{(m)}(z) = \frac{\cosh\big(k_0^{(m)}(z+h_m)\big)}{\cosh\big(k_0^{(m)}h_m\big)},$$

$$Z_n^{(m)}(z) = \frac{\cos\big(k_n^{(m)}(z+h_m)\big)}{\cos\big(k_n^{(m)}h_m\big)}, \quad n=1, 2, \ldots, \quad m=1, 3. \tag{2.10b}$$

It is important to observe that the wavenumbers $\{\mathrm{i}k_0^{(m)}, k_n^{(m)}, n=1, 2, \ldots\}$ and the vertical eigenfunctions $\{Z_n^{(m)}(z), n=0, 1, 2, \ldots\}$, $m=1, 3$, are ξ-independent.

By invoking the standard theory of regular eigenvalue problems (see e.g. Coddington & Levinson 1955, § 7.4), we can assert that the expansions (2.7*a*, *b*) are complete in the intervals $z\in[-h_m, 0]$, $m=1, 3$, respectively. Thus, under the assumption that the functions $\{C_n^{(m)}(\xi), n=0, 1, 2\ldots\}$, $m=1, 3$, are absolutely integrable on the real axis $\xi\in R$, all requirements of the transformed problem $\mathscr{P}_\xi(D, \mu, \boldsymbol{x}_0)$ are fulfilled in $D^{(m)}$, $m=1, 3$, respectively, including the radiation condition, (2.5*d*).

Exploiting the expansions (2.7) the problem $\mathscr{P}_\xi(D, \mu, \boldsymbol{x}_0)$ can be reformulated as a matching-boundary value problem in the bounded subdomain $D^{(2)}$ as follows:

Problem $\mathscr{P}_\xi^T(D^{(2)}, C_n^{(1)}, C_n^{(3)}, \mu, \boldsymbol{x}_0)$: Find the potential $\varphi^{(2)}(x, z; \xi)$ defined in $D^{(2)}$, and the coefficients $C_n^{(m)}(\xi)$, $m=1, 3$, $n=0, 1, 2, \ldots$, satisfying the equations

$$\nabla^2\varphi^{(2)} - \xi^2\varphi^{(2)} = -\frac{1}{2\pi}\delta(x-x_0)\delta(z-z_0), \quad \boldsymbol{x}\in D^{(2)}, \tag{2.11a}$$

$$\frac{\partial\varphi^{(2)}}{\partial z} - \mu\varphi^{(2)} = 0, \quad \boldsymbol{x}\in\partial D_F^{(2)}, \quad \frac{\partial\varphi^{(2)}}{\partial n} = 0, \quad \boldsymbol{x}\in\partial D_\Pi^{(2)}, \tag{2.11b, c}$$

$$\varphi^{(2)} = \varphi^{(1)}, \quad \frac{\partial\varphi^{(2)}}{\partial x} = \frac{\partial\varphi^{(1)}}{\partial x}, \quad \boldsymbol{x}\in\partial D_I^{(12)}, \tag{2.11d, e}$$

$$\varphi^{(2)} = \varphi^{(3)}, \quad \frac{\partial\varphi^{(2)}}{\partial x} = \frac{\partial\varphi^{(3)}}{\partial x}, \quad \boldsymbol{x}\in\partial D_I^{(23)}, \tag{2.11f, g}$$

where $\boldsymbol{n}$ denotes the outward unit normal vector; see figure 1. The wave potentials $\varphi^{(m)}$, $m=1, 3$, and their horizontal derivatives $\partial\varphi^{(m)}/\partial x$, appearing in the above equations are considered to be defined through the series expansions (2.7), and their termwise derivatives with respect to the horizontal coordinate, at $x=a$ and $x=b$, respectively.

2.3. *Extension of the formulation to complex* ξ

To obtain the numerical solution of the original problem $\mathscr{P}_{3D}(D_{3D}, \mu, \boldsymbol{r}_0)$, the Fourier inversion (2.4*b*) will be evaluated by an efficient application of the discrete Fourier transform (described in § 5). The discrete Fourier transform is based on the truncation of the infinite interval of integration and on the discretization (sampling) of the integrand in the finite subinterval. However, it is well known that undersampling in the ξ-domain causes aliasing in the physical y-domain. An effective way to eliminate the aliasing problem is to move the integration contour into the complex plane. Thus, we need to consider the transformed wave problem for $\xi=\xi_1+\mathrm{i}\xi_2$. Under specific conventions that will be introduced below for restoring the analyticity in the complex domain of the multi-valued functions $\mathscr{K}_n^{(m)}(\xi)$, $n=0, 1, 2, \ldots$, $m=1, 3$, defined by (2.8), it can be seen that the representations (2.7) remain valid for ξ lying in the two

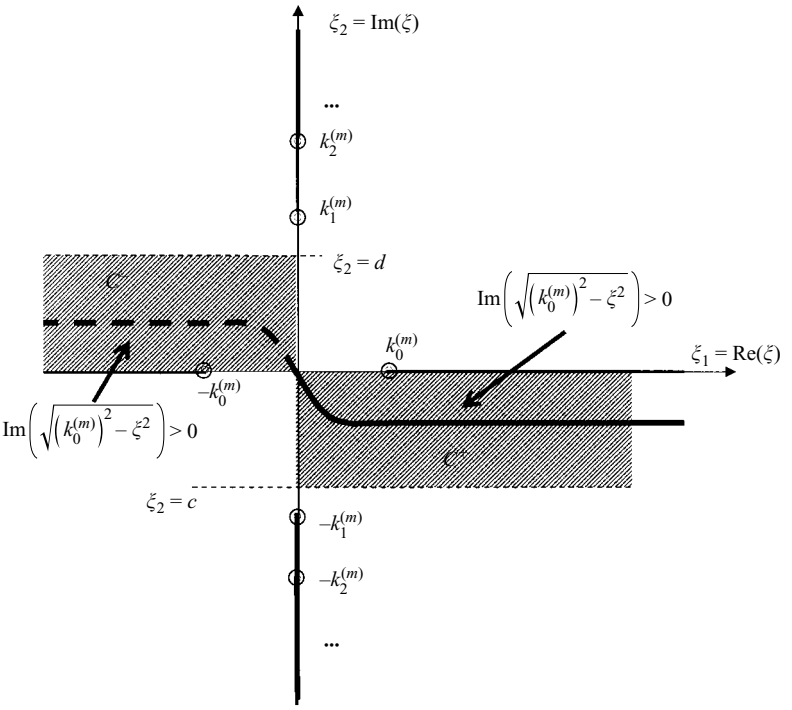

FIGURE 2. The strips S_{c0}^+ and S_{0d}^- and the contour of integration $C = C^- \cup C^+$ for the Fourier inversion in the complex ξ-domain. The location of the singularities $\pm k_0^{(m)}, \pm \mathrm{i}k_1^{(m)}, \pm \mathrm{i}k_2^{(m)}, \ldots,$ and the associated branch cuts, for each half-strip $D^{(m)}, m = 1, 3$, is shown by using small circles and thick lines, respectively. Note that the path of integration is selected to pass through the strips S_{c0}^+ and S_{0d}^-, where $\mathrm{Im}(\sqrt{(k_0^{(m)})^2 - \xi^2}) > 0$.

half-strips:

$$\xi \in S_{c0}^+ = \{0 < \xi_1 < \infty, c \leqslant \xi_2 < 0\}, \quad \text{where} \quad -\min\left\{k_1^{(1)}, k_1^{(3)}\right\} < c \leqslant 0, \quad (2.12a)$$

and

$$S_{0d}^- = \{-\infty < \xi_1 < 0, 0 < \xi_2 \leqslant d\}, \quad \text{where} \quad 0 \leqslant d < \min\left\{k_1^{(1)}, k_1^{(3)}\right\}. \quad (2.12b)$$

These strips are shown in figure 2 (shaded area). The branch points of the functions $\mathscr{K}_0^{(m)}(\xi) = \sqrt{(k_0^{(m)})^2 - \xi^2}$, are located symmetrically on the real ξ-axis at the points $\xi = \pm k_0^{(m)}$, $m = 1, 3$. We define the associated cuts along the real ξ-axis, as presented in figure 2 (thick lines), so that the imaginary part of $\mathscr{K}_0^{(m)}(\xi)$ takes positive values below the positive real axis and above the negative real axis. Thus, for $\xi \in S_{c0}^+ \cup S_{0d}^-$, the following holds: $\mathrm{Im}\{\mathscr{K}_0^{(m)}(\xi)\} > 0$. In addition, the branch points of the functions $\mathscr{K}_n^{(m)}(\xi) = \sqrt{(k_n^{(m)})^2 + \xi^2}$, $n = 1, 2 \ldots, m = 1, 3$, are located symmetrically on the imaginary ξ-axis at the points $\xi = \pm \mathrm{i}k_n^{(m)}, n = 1, 2 \ldots, m = 1, 3$. We define the associated cuts along the imaginary ξ-axis, as presented in figure 2, so that $\mathrm{Re}\{\mathscr{K}_n^{(m)}(\xi)\} > 0$ for $\xi \in S_{c0}^+ \cup S_{0d}^-$.

On the basis of the above considerations, and under the assumptions that the functions $\{C_n^{(m)}(\xi), n = 0, 1, 2 \ldots\}$, $m = 1, 3$, are analytic in $S_{c0}^+ \cup S_{0d}^-$, and satisfy the

following growth conditions, for $\xi \in S_{c0}^{+} \cup S_{0d}^{-}$, $|\xi_1| \to \infty$:

(i) $\left|C_0^{(1)}(\xi)\right| < A_0^{(1)} \exp\left(-a \mathrm{Im}\left\{\mathscr{K}_0^{(1)}(\xi)\right\}\right), \quad \left|C_0^{(3)}(\xi)\right| < A_0^{(3)} \exp\left(b \mathrm{Im}\left\{\mathscr{K}_0^{(m)}(\xi)\right\}\right),$

(ii) $\left|C_n^{(m)}(\xi)\right| < A_n^{(m)}(1 + |\xi|^q), \quad$ for some $q > 0,$

where $A_n^{(m)}$, $n = 0, 1, 2, \ldots$, $m = 1, 3$, are positive constants, the representations (2.7) satisfy all the requirements of the transformed problem $\mathscr{P}_\xi(D, \mu, \boldsymbol{x}_0)$ in $D^{(m)}$, $m = 1, 3$, respectively, including the radiation condition, (2.5*d*). Moreover, in accordance with the above conventions, the condition of symmetry (2.6) is naturally extended into the complex domain, and thus the transformed problem $\mathscr{P}_\xi(D, \mu, \boldsymbol{x}_0)$ is expected to be symmetric with respect to the origin, i.e.

$$\varphi(\boldsymbol{x}, \boldsymbol{x}_0; \xi_1 + \mathrm{i}\xi_2) = \varphi(\boldsymbol{x}, \boldsymbol{x}_0; -\xi_1 - \mathrm{i}\xi_2), \quad \xi \in S_{c0}^{+}. \tag{2.13}$$

On the basis of the theory of analytic functions, see, e.g., Sidorov, Fedoryuk & Shabunin (1985), the Fourier inversion can now be equivalently calculated by moving the integration contour (C) in the complex domain within $S_{c0}^{+} \cup S_{0d}^{-}$. Furthermore, by taking the contour to be symmetric with respect to the origin, see figure 2, and using (2.13), the Fourier inversion is written as follows:

$$\Phi(\boldsymbol{r}, \boldsymbol{r}_0; \mu) = 2 \int_{\xi \in (C^+)} \varphi(\boldsymbol{x}, \boldsymbol{x}_0; \xi) \cos(\xi y) \, \mathrm{d}\xi, \tag{2.14}$$

where (C^+) is the part of (C) lying in S_{c0}^{+}.

3. The treatment of the physical-space singularity

3.1. *Decomposition of the wave potential into singular and regular parts*

The potentials $\Phi(\boldsymbol{r}, \boldsymbol{r}_0; \mu)$ in three dimensions, and $\varphi(\boldsymbol{x}, \boldsymbol{x}_0; \xi)$ in two dimensions, exhibit, respectively, the singularities

$$\Phi(\boldsymbol{r}, \boldsymbol{r}_0; \mu) \sim \frac{1}{4\pi |\boldsymbol{r} - \boldsymbol{r}_0|} \quad \text{as} \quad \boldsymbol{r} \to \boldsymbol{r}_0, \tag{3.1a}$$

and

$$\varphi(\boldsymbol{x}, \boldsymbol{x}_0; \xi) \sim K_0(\xi |\boldsymbol{x} - \boldsymbol{x}_0|)/(2\pi)^2 \quad \text{as} \quad \boldsymbol{x} \to \boldsymbol{x}_0 \quad \text{for} \quad \xi \in R^+, \tag{3.1b}$$

where K_0 is the Bessel-K function of zero order. Therefore, it is natural, to seek a decomposition of the solution of the problem $\mathscr{P}_\xi^T(D^{(2)}, C_n^{(1)}, C_n^{(3)}, \mu, \boldsymbol{x}_0)$ of the form

$$\varphi^{(2)}(\boldsymbol{x}, \boldsymbol{x}_0; \xi) = \varphi_{sng}(\boldsymbol{x}, \boldsymbol{x}_0; \xi) + \varphi_{reg}(\boldsymbol{x}, \boldsymbol{x}_0; \xi), \quad \boldsymbol{x} \in D^{(2)}, \tag{3.2}$$

where $\varphi_{sng}(\boldsymbol{x}, \boldsymbol{x}_0; \xi)$ contains the singularity (3.1*b*), and $\varphi_{reg}(\boldsymbol{x}, \boldsymbol{x}_0; \xi)$ remains regular throughout the whole physical domain $D^{(2)}$. For reasons that will be explained below, in the present work, the singular part of the solution is selected to be of the form

$$\varphi_{sng}(\boldsymbol{x}, \boldsymbol{x}_0; \xi) = c(\boldsymbol{x}, \boldsymbol{x}_0) \frac{K_0(\xi |\boldsymbol{x} - \boldsymbol{x}_0|)}{(2\pi)^2} + A(\boldsymbol{x}, \boldsymbol{x}_0; \xi), \tag{3.3}$$

where $c(\boldsymbol{x}, \boldsymbol{x}_0)$ and $A(\boldsymbol{x}, \boldsymbol{x}_0; \xi)$ are regular functions, and $c(\boldsymbol{x}_0, \boldsymbol{x}_0) = 1$. It is useful to make a distinction here between the physical-space singularity, located at $\boldsymbol{x} = \boldsymbol{x}_0$, and the singularities that both $\varphi_{sng}(\boldsymbol{x}, \boldsymbol{x}_0; \xi)$ and $\varphi_{reg}(\boldsymbol{x}, \boldsymbol{x}_0; \xi)$ may have in the complex ξ-plane. Let Ξ denote the set of points in the strip S_{c0}^{+} at which $\varphi_{sng}(\boldsymbol{x}, \boldsymbol{x}_0; \xi)$ or $\varphi_{reg}(\boldsymbol{x}, \boldsymbol{x}_0; \xi)$ may become singular. Then, for all $\xi \in S_{c0}^{+} \backslash \Xi$ (called also ξ-regular values), the function $\varphi_{reg}(\boldsymbol{x}, \boldsymbol{x}_0; \xi)$ is considered to be bounded and smooth (at

least twice continously differentiable) with respect to both physical-space coordinates $\boldsymbol{x}, \boldsymbol{x}_0 \in D$.

The two functions φ_{sng} and φ_{reg} need not satisfy individually the differential equation and all the boundary/matching conditions of the problem. All these requirements are to be fulfilled by their superposition (3.2). Apart from its singular character, the following additional requirements are imposed on φ_{sng}:

(i) to satisfy individually the free-surface condition

$$\frac{\partial \varphi_{sng}}{\partial z} - \mu \varphi_{sng} = 0, \quad \boldsymbol{x} \in \partial D_F, \tag{3.4a}$$

and

(ii) to vanish identically in a neighbourhood of the vertical interfaces $\partial D^{(12)}$, $\partial D^{(23)}$, i.e.

$$\varphi_{sng}(\boldsymbol{x}, \boldsymbol{x}_0; \xi) = 0 \quad \begin{cases} \text{for } x \in [a, a+\delta), & z \in [-h(a), 0], \\ \text{for } x \in (b-\delta, b], & z \in [-h(b), 0], \end{cases} \tag{3.4b}$$

where $\delta > 0$. The latter requirement implies

$$\varphi_{reg}(\boldsymbol{x}, \boldsymbol{x}_0; \xi) = \varphi^{(1)}(\boldsymbol{x}, \boldsymbol{x}_0; \xi) \quad \text{and} \quad \frac{\partial \varphi_{reg}(\boldsymbol{x}, \boldsymbol{x}_0; \xi)}{\partial x} = \frac{\partial \varphi^{(1)}(\boldsymbol{x}, \boldsymbol{x}_0; \xi)}{\partial x}, \quad \boldsymbol{x} \in \partial D_I^{(12)}, \tag{3.5a, b}$$

and similar matching conditions on $\partial D_I^{(23)}$. That is, the satisfaction of the matching conditions on the vertical interfaces is taken over by φ_{reg} only, which simplifies the corresponding numerical implementation.

Requirement (i), (3.4*a*), implies that $\varphi_{reg}(\boldsymbol{x}, \boldsymbol{x}_0; \xi)$ must also satisfy the free-surface condition

$$\frac{\partial \varphi_{reg}}{\partial z} - \mu \varphi_{reg} = 0 \quad \text{at} \quad \boldsymbol{x} \in \partial D_F. \tag{3.6}$$

The above facts will greatly facilitate our treatment later on.

3.2. *Construction of* $\varphi_{sng}(\boldsymbol{x}, \boldsymbol{x}_0; \xi)$

First, we consider the free-space Green's function of the two-dimensional modified Helmholtz operator $\nabla^2 - \xi^2$,

$$G(\boldsymbol{x}, \boldsymbol{x}_0; \xi) = \frac{1}{(2\pi)^2} K_0(\xi |\boldsymbol{x} - \boldsymbol{x}_0|) = \frac{\mathrm{i}}{8\pi} H_0^{(1)}(\mathrm{i}\xi |\boldsymbol{x} - \boldsymbol{x}_0|), \tag{3.7}$$

where $H_0^{(1)}(\cdot)$ is the Hankel function of first kind and zero order. It should be noted that $G(\boldsymbol{x}, \boldsymbol{x}_0; \xi)$, as given by (3.7), remains valid for complex $\xi \in S_{c0}^{+}$. See e.g. Noble (1958), or Vladimirov (1984).

Consider also the reduced wave potential associated with $G(\boldsymbol{x}, \boldsymbol{x}_0; \xi)$, defined by (see e.g. Wehausen & Laitone 1960, § 18)

$$F(\boldsymbol{x}, \boldsymbol{x}_0; \xi) = \frac{\partial G(\boldsymbol{x}, \boldsymbol{x}_0; \xi)}{\partial z} - \mu G(\boldsymbol{x}, \boldsymbol{x}_0; \xi), \quad \boldsymbol{x}_0 \in D^{(2)}. \tag{3.8}$$

Assuming now that $\boldsymbol{x}_0 \in D^{(2)}$ is a strictly interior point of the variable-bathymetry subdomain, the restriction of the reduced potential on the free surface

$$F_0(\boldsymbol{x}, \boldsymbol{x}_0; \xi) = \frac{\partial G(x, z=0, \boldsymbol{x}_0; \xi)}{\partial z} - \mu G(x, z=0, \boldsymbol{x}_0; \xi), \quad a \leqslant x \leqslant b, \tag{3.9}$$

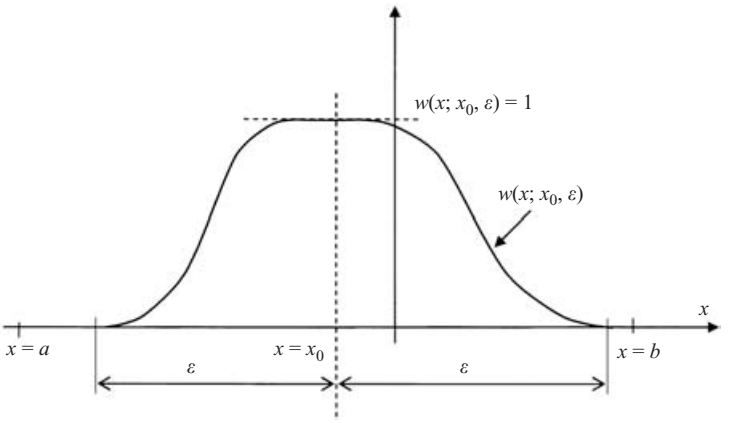

FIGURE 3. The filter function $w(x;x_0,\varepsilon)=\tilde{w}(|x-x_0|/\varepsilon)$.

constitutes a smooth (differentiable) function of the horizontal coordinate x. By using (3.9) and (3.7), we obtain the following explicit form of $F_0(\boldsymbol{x},\boldsymbol{x}_0;\xi)$:

$$F_0(\boldsymbol{x},\boldsymbol{x}_0;\xi)=\frac{1}{(2\pi)^2}\left(\frac{z_0}{x_F}\xi K_1(\xi x_F)-\mu K_0(\xi x_F)\right), \tag{3.10}$$

where $x_F=\sqrt{(x-x_0)^2+z_0^2}$ is the distance of any point on the free surface $\boldsymbol{x}=(x,0)\in\partial D_F$ from the source point (x_0,z_0). Since $F_0(\boldsymbol{x},\boldsymbol{x}_0;\xi)$ is z-independent and satisfies (3.9), it is easily seen that the potential

$$\varphi_{sng}(\boldsymbol{x},\boldsymbol{x}_0;\xi)=\left(G(\boldsymbol{x},\boldsymbol{x}_0;\xi)+\frac{1}{\mu}F_0(\boldsymbol{x},\boldsymbol{x}_0;\xi)\right)w(x;x_0,\varepsilon),\quad \xi\in S^+_{c0}, \tag{3.11}$$

satisfies the free-surface condition (3.4*a*). The function $w(x;x_0,\varepsilon)$ is a ξ- and z-independent, smooth, one-dimensional function, centred at the horizontal position of the source, $x=x_0$, which is introduced in order to make possible the satisfaction of condition (3.4*b*). It is taken to be an even function of the form

$$w(x;x_0,\varepsilon)=\begin{cases}\tilde{w}\left(\dfrac{|x-x_0|}{\varepsilon}\right), & |x-x_0|\leqslant\varepsilon\\ 0, & |x-x_0|>\varepsilon,\end{cases} \tag{3.12}$$

where $\tilde{w}(t)$, $t\in R^+$, is a filter function, similar to a mollifier, Oden & Reddy (1976). See figure 3. In order that the function $\varphi_{sng}(\boldsymbol{x},\boldsymbol{x}_0;\xi)$, as defined by (3.11), satisfies (3.4*b*), the filter function $\tilde{w}(t)$ must fulfil the following conditions:

(i) the scale parameter ε should satisfy the inequality

$$\varepsilon<\min\{|b-x_0|,|a-x_0|\}; \tag{3.13a}$$

(ii) $\tilde{w}(t)$ must be smooth, at least twice continuously differentiable in R^+;

(iii)

$$\tilde{w}(0)=1,\quad \tilde{w}'(0)=\tilde{w}''(0)=0,\quad \text{and}\quad \tilde{w}(1)=\tilde{w}'(1)=\tilde{w}''(1)=0, \tag{3.13b}$$

where a prime denotes differentiation with respect to t. The necessity of the conditions (3.13*b*) will be further explained in the next subsection.

There are many choices for the shape of the filter function. Two particular filters, that will also be used for obtaining numerical results, are the exponential filter

$$\tilde{w}(t) = \exp\left(- \frac{t^3}{1-t^3} \right), \quad 0 \leqslant t \leqslant 1, \tag{3.14a}$$

and the polynomial filter

$$\tilde{w}(t) = -0.5t^6 - 4.5t^5 + 13.5t^4 - 9.5t^3 + 1, \quad 0 \leqslant t \leqslant 1. \tag{3.14b}$$

By comparing (3.11) and (3.3), we immediately see that $c(\boldsymbol{x}, \boldsymbol{x}_0) = w(\boldsymbol{x}; \boldsymbol{x}_0, \varepsilon)$ and $A(\boldsymbol{x}, \boldsymbol{x}_0; \xi) = (1/\mu) w(\boldsymbol{x}, \boldsymbol{x}_0; \varepsilon) F_0(\boldsymbol{x}, \boldsymbol{x}_0; \xi)$. This completes the construction of the singular part of the wave potential, in the form (3.3).

3.3. *Properties of the singular part* $\varphi_{sng}(\boldsymbol{x}, \boldsymbol{x}_0; \xi)$

A very important property of $\varphi_{sng}(\boldsymbol{x}, \boldsymbol{x}_0; \xi)$, as defined by (3.11) for $\xi \in S_{c0}^{+}$ and extended by (2.13) to S_{0d}^{-}, is that its inverse Fourier transform can be analytically calculated and easily evaluated. Other choices are also possible, e.g. the deep-water harmonic-source potential in combination with the filter function, but the singular part obtained in the physical space is more difficult to evaluate, e.g. it is given through a wavenumber integral. The present choice has the advantage that its inverse Fourier transform is obtained in a simple closed form. In fact, since $\varphi_{sng}(\boldsymbol{x}, \boldsymbol{x}_0; \xi)$ is ξ-analytic in S_{c0}^{+}, and satisfies property that $\varphi_{sng}(\boldsymbol{x}, \boldsymbol{x}_0; \xi) \to 0$ as $\xi_1 \to \infty$, where $\xi = \xi_1 + \mathrm{i}\xi_2 \in S_{c0}^{+}$, we obtain (cf. (2.14)):

$$\begin{aligned} \Phi_{sng}(\boldsymbol{r}, \boldsymbol{r}_0, \mu) &= \int_{-\infty}^{0} \varphi_{sng}(\boldsymbol{x}, \boldsymbol{x}_0; \xi_1 + 0\mathrm{i}) \exp(\mathrm{i}y\xi_1)\, \mathrm{d}\xi_1 \\ &\quad + \int_{0}^{+\infty} \varphi_{sng}(\boldsymbol{x}, \boldsymbol{x}_0; \xi_1 - 0\mathrm{i}) \exp(\mathrm{i}y\xi_1)\, \mathrm{d}\xi_1 \\ &= 2 \int_{0}^{+\infty} \varphi_{sng}(\boldsymbol{x}, \boldsymbol{x}_0; \xi_1 - 0\mathrm{i}) \cos(y\xi_1)\, \mathrm{d}\xi_1 \\ &= \tilde{w}\left(\frac{|x - x_0|}{\varepsilon} \right) \left(\frac{1}{4\pi r} + \frac{1}{4\pi r_F} \left(\frac{z_0}{\mu r_F^2} - 1 \right) \right), \end{aligned} \tag{3.15a}$$

where

$$r = \sqrt{(x-x_0)^2 + y^2 + (z-z_0)^2}, \quad r_F = \sqrt{(x-x_0)^2 + y^2 + z_0^2}. \tag{3.15b}$$

The inversion (3.15) is obtained by using the results in Gradshteyn & Ryzhik (1965, par. 6.671/14 and 6.699/12), concerning the Fourier integrals of $K_0(\xi x_F)$ and $\xi K_1(\xi x_F)$ over the positive real axis. Let us now list the other important properties of $\varphi_{sng}(\boldsymbol{x}, \boldsymbol{x}_0; \xi)$:

(i) By virtue of the cut-off character of the filter function w, the singular part of the transformed wave potential, φ_{sng}, becomes identically zero in the neighbourhood of the two vertical interfaces $\partial D_I^{(12)}$ and $\partial D_I^{(23)}$, thus rendering valid both 3.5(a) and (3.5b).

(ii) By assumptions (3.13b) and the property that $F_0(\boldsymbol{x}, \boldsymbol{x}_0; \xi)$ is regular in physical space, the function $\varphi_{sng}(\boldsymbol{x}, \boldsymbol{x}_0; \xi)$ exhibits exactly the same singularity as the free-space Green's function $G(\boldsymbol{x}, \boldsymbol{x}_0; \xi)$. More precisely, for $\boldsymbol{x} \in D^{(2)}$, straightforward calculation leads to the following result:

$$(\nabla^2 - \xi^2)\varphi_{sng} = -\frac{1}{2\pi} \delta(x - x_0)\delta(z - z_0) + g(\boldsymbol{x}, \boldsymbol{x}_0; \xi), \tag{3.16a}$$

where

$$g(\boldsymbol{x}, \boldsymbol{x}_0; \xi) = g_1(\boldsymbol{x}, \boldsymbol{x}_0; \xi) + g_2(\boldsymbol{x}, \boldsymbol{x}_0; \xi), \tag{3.16b}$$

$$g_1(\boldsymbol{x}, \boldsymbol{x}_0; \xi) = G\frac{\partial^2 w}{\partial x^2} + 2\frac{\partial G}{\partial x}\frac{\partial w}{\partial x}, \tag{3.16c}$$

$$g_2(\boldsymbol{x}, \boldsymbol{x}_0; \xi) = \left(\frac{\partial^2 F_0}{\partial x^2} - \xi^2 F_0\right)\frac{w}{\mu} + \frac{2}{\mu}\frac{\partial F_0}{\partial x}\frac{\partial w}{\partial x} + \frac{F_0}{\mu}\frac{\partial^2 w}{\partial x^2}. \tag{3.16d}$$

Both functions $g_1(\boldsymbol{x}, \boldsymbol{x}_0; \xi)$ and $g_2(\boldsymbol{x}, \boldsymbol{x}_0; \xi)$, as defined by the above equations, are continuous throughout $D^{(2)}$. This is obvious for g_2, since all of its components are regular functions of x. In the case of g_1, which contains the free-space Green's function and its first derivative, the regularization is achieved by the action of the filter function and its derivatives at $x = x_0$. These observations justify the requirements (3.13*b*) imposed on the shape of the filter function.

3.4. *The matching-boundary value problem for* $\varphi_{reg}(x, z; \xi)$

On the basis of all the above results, and using the decomposition (3.2), the matching-boundary value problem $\mathscr{P}_\xi^T(D^{(2)}, C_n^{(1)}, C_n^{(3)}, \mu, \boldsymbol{x}_0)$ can be equivalently reformulated as a problem on the regular part of the transformed wave potential $\varphi_{reg}(\boldsymbol{x}, \boldsymbol{x}_0; \xi)$ in the bounded subdomain $D^{(2)}$ as follows:

Regularized reformulation of problem $\mathscr{P}_\xi^T(D^{(2)}, C_n^{(1)}, C_n^{(3)}, \mu, \boldsymbol{x}_0)$: find the function $\varphi_{reg}(x, z; \xi)$, defined in $D^{(2)}$, and the coefficients $C_n^{(m)}(\xi)$, $n = 0, 1, 2, \ldots$, of the expansions (2.7) of $\varphi^{(m)}(x, z; \xi)$, $m = 1, 3$, satisfying the equations

$$\nabla^2\varphi_{reg} - \xi^2\varphi_{reg} = -g(\boldsymbol{x}, \boldsymbol{x}_0, \xi), \qquad \boldsymbol{x} \in D^{(2)}, \tag{3.17a}$$

$$\frac{\partial\varphi_{reg}}{\partial z} - \mu\varphi_{reg} = 0, \qquad \boldsymbol{x} \in \partial D_F^{(2)}, \tag{3.17b}$$

$$\frac{\partial\varphi_{reg}}{\partial n} = -\frac{\partial\varphi_{sng}}{\partial n} \equiv f(\boldsymbol{x}, \boldsymbol{x}_0, \xi), \qquad \boldsymbol{x} \in \partial D_\Pi^{(2)}, \tag{3.17c}$$

$$\varphi_{reg} = \varphi^{(1)}, \quad \frac{\partial\varphi_{reg}}{\partial x} = \frac{\partial\varphi^{(1)}}{\partial x}, \qquad \boldsymbol{x} \in \partial D_I^{(12)}, \tag{3.17d, e}$$

$$\varphi_{reg} = \varphi^{(3)}, \quad \frac{\partial\varphi_{reg}}{\partial x} = \frac{\partial\varphi^{(3)}}{\partial x}, \qquad \boldsymbol{x} \in \partial D_I^{(23)}. \tag{3.17f, g}$$

The forcing of the above problem is two-fold:

(i) the forcing-term $g(\boldsymbol{x}, \boldsymbol{x}_0; \xi)$ appearing on the right-hand side of the field equation (3.17*a*), which is given by (3.16), and

(ii) the forcing-term appearing on the right-hand side of the bottom boundary condition (3.17*c*), given by

$$f(\boldsymbol{x}, \boldsymbol{x}_0; \xi) \equiv -\frac{\partial\varphi_{sng}}{\partial n} = \left(\frac{\partial}{\partial z} + h'(x)\frac{\partial}{\partial x}\right)\varphi_{sng}(x, z = -h(x); \xi), \qquad \boldsymbol{x} \in \partial D_\Pi^{(2)}. \tag{3.18a}$$

Using (3.11), (3.18*a*) takes the form

$$f(x, \boldsymbol{x}_0; \xi) = w\left\{\frac{\partial G}{\partial z} + h'(x)\left(\frac{\partial G}{\partial x} + \frac{1}{\mu}\frac{\partial F_0}{\partial x}\right)\right\}_{z=-h(x)} + \frac{\partial w}{\partial x}\left(G + \frac{F}{\mu}\right)_{z=-h(x)}. \tag{3.18b}$$

One important feature of problem (3.17) is that it involves the regular forcing terms f and g instead of the singular δ-type forcing of the problem (2.11). Thus, it admits regular solutions, which are much more amenable to accurate numerical treatment. Also, due to the specific form of $\varphi_{sng}(\boldsymbol{x}, \boldsymbol{x}_0; \xi)$, the regularized part $\varphi_{reg}(x, z; \xi)$ should satisfy the homogeneous free-surface condition, (3.17b), and the same type of (unforced) matching conditions, (3.17d, e) and (3.17f, g), on the vertical interfaces $\partial D_I^{(12)}$ and $\partial D_I^{(23)}$, respectively, like problem (2.11). These facts make the problem (3.17) quite similar with the corresponding propagation problem treated by Athanassoulis & Belibassakis (1999). Thus, the method of numerical solution developed for the latter can be easily implemented for the present problem, with appropriate modifications.

4. The variational principle and the coupled-mode system of equations

4.1. *The variational principle*

Problem (3.17) admits a variational formulation in accordance with a similar construction for the corresponding water-wave propagation problem. The variational principle and its application to the derivation of an equivalent coupled-mode system of equations will be outlined in this section.

Consider the functional $\mathscr{F}_\xi = \mathscr{F}_\xi(\varphi_{reg}, \{C_n^{(1)}\}_{n=0,1,\ldots}, \{C_n^{(3)}\}_{n=0,1,\ldots})$ defined by

$$\mathscr{F}_\xi = \frac{1}{2}\int_{D^{(2)}} [(\nabla\varphi_{reg})^2 + \xi^2(\varphi_{reg})^2 - g\varphi_{reg}]\,\mathrm{d}x\,\mathrm{d}z - \tfrac{1}{2}\mu\int_{\partial D_F^{(2)}} (\varphi_{reg})^2\,\mathrm{d}x - \int_{\partial D_\Pi^{(2)}} f\varphi_{reg}\,\mathrm{d}s + \int_{\partial D_I^{(12)}} \big(\varphi_{reg} - \tfrac{1}{2}\varphi^{(1)}\big)\frac{\partial\varphi^{(1)}}{\partial x}\,\mathrm{d}z - \int_{\partial D_I^{(23)}} \big(\varphi_{reg} - \tfrac{1}{2}\varphi^{(3)}\big)\frac{\partial\varphi^{(3)}}{\partial x}\,\mathrm{d}z, \quad (4.1)$$

where $\mathrm{d}s$ is the surface differential over $\partial D_\Pi^{(2)}$. The left- and right-hand half-strip wave potentials $\varphi^{(1)}, \varphi^{(3)}$, appearing in (4.1), are considered only on the interfaces $\partial D_I^{(12)}, \partial D_I^{(23)}$, respectively. Moreover, because of the expansions (2.7a, b), these potentials are equivalently described by means of the corresponding coefficients $\{C_n^{(m)}\}_{n=0,1,2\ldots}$, $m = 1, 3$. This observation explains why the arguments of the functional $\mathscr{F}_\xi$ are taken to be $(\varphi_{reg}, \{C_n^{(1)}\}_{n=0,1,\ldots}, \{C_n^{(3)}\}_{n=0,1,\ldots})$. It should also be noted that the above functional is parametrically dependent on the complex Fourier parameter ξ. This dependence comes not only through the term with integrand $\xi^2(\varphi_{reg})^2$, but also through the ξ-dependence of the functions g, equation (3.16), f, equation (3.18), and $\varphi^{(m)}$, $\{C_n^{(m)}\}_{n=0,1,2,\ldots}$, $m = 1, 3$, equation (2.7).

The variational principle of the problem (3.17) is now stated as follows:

Theorem A: *The variational principle of problem (3.17). For any given $\xi \in S_{d0}^+ \backslash \Xi$, the functions $\varphi_{reg}(x, z; \xi)$ in $D^{(2)}$, and $\varphi^{(m)}(x, z; \{C_n^{(m)}(\xi)\}_{n=0,1,\ldots}; \xi)$ in $D^{(m)}$, $m = 1, 3$, form a solution of the matching-boundary value problem (3.17), if and only if they render the functional $\mathscr{F}_\xi$ stationary, i.e. iff they satisfy the variational equation*

$$\delta\mathscr{F}_\xi\big(\varphi_{reg}, \{C_n^{(1)}\}_{n=0,1,\ldots}, \{C_n^{(3)}\}_{n=0,1,\ldots}\big) = 0. \quad (4.2a)$$

The proof follows the lines of the proof of a similar principle concerning the corresponding propagation problem; see Athanassoulis & Belibassakis (1999) and the references cited there. We only note here that, by calculating the first variation $\delta\mathscr{F}_\xi$ of the functional, and using Green's theorem, the variational equation (4.2a)

takes the form

$$-\int_{D^{(2)}}(\nabla^2\varphi_{reg}-\xi^2\varphi_{reg}+g)\delta\varphi_{reg}\,\mathrm{d}x\,\mathrm{d}z+\int_{\partial D_{\Pi}^{(2)}}\left(\frac{\partial\varphi_{reg}}{\partial n^{(2)}}-f\right)\delta\varphi_{reg}\,\mathrm{d}s$$
$$+\int_{\partial D_F^{(2)}}\left(\frac{\partial\varphi_{reg}}{\partial z}-\mu\varphi_{reg}\right)\delta\varphi_{reg}\,\mathrm{d}x-\int_{\partial D_I^{(12)}}\left(\frac{\partial\varphi_{reg}}{\partial x}-\frac{\partial\varphi^{(1)}}{\partial x}\right)\partial\varphi_{reg}\,\mathrm{d}z$$
$$+\int_{\partial D_I^{(23)}}\left(\frac{\partial\varphi_{reg}}{\partial x}-\frac{\partial\varphi^{(3)}}{\partial x}\right)\delta\varphi_{reg}\,\mathrm{d}z+\int_{\partial D_I^{(12)}}(\varphi_{reg}-\varphi^{(1)})\delta\left(\frac{\partial\varphi^{(1)}}{\partial x}\right)\mathrm{d}z$$
$$-\int_{\partial D_I^{(23)}}(\varphi_{reg}-\varphi^{(3)})\delta\left(\frac{\partial\varphi^{(3)}}{\partial x}\right)\mathrm{d}z=0. \tag{4.2b}$$

Thus, invoking the standard arguments of the Calculus of Variations, we readily obtain the equivalence of the variational equation (4.2*b*) and the problem (3.17).

Using the above variational equation, in conjunction with any consistent representation for the admissible function φ_{reg}, permits us to obtain an equivalent set of equations for the matching-boundary value problem.

4.2. *A consistent local-mode representation of the transformed wave potential in* $D^{(2)}$

The above variational principle will now be used to obtain an alternative, semi-discrete formulation φ_{reg} in $D^{(2)}$, in the form of a system of horizontal differention equations. This reformulation is based on the representation of the admissible field $\varphi_{reg}(x,z,\xi)$ in terms of modal fields of the form $\varphi_n(x;\xi)Z_n(z;x)$. (The set of admissible functions $\varphi_{reg}(x,z)$ is the set $C^2(D^{(2)})\cap C^1(\overline{D^{(2)}})$, i.e. the set of functions being twice continuously differentiable at all interior points of $D^{(2)}$, having continuous derivatives up to the boundary). The ξ-independent functions $Z_n(z;x)$, $a\leqslant x\leqslant b$, are obtained (except one of them which will be discussed separately) by means of a local vertical Sturm–Liouville problem of the form (2.9) in the z-interval $[-h(x),0]$. The form of functions $Z_n(z;x)$, $n=0,1,2,\ldots$, is similar to (2.10*b*), with h_m and $k_n^{(m)}$, $n=0,1,2,\ldots$, being replaced by the local depth $h(x)$, and the local eigenvalues $k_n(x)$, $n=0,1,2,\ldots$, respectively. The latter are obtained as the roots of the local dispersion relation

$$\mu h_i(x)=-k(x)h(x)\tan[k(x)h(x)],\quad a\leqslant x\leqslant b. \tag{4.3a}$$

The above set of local modes (propagating and evanescent) is completed by an additional mode, called the *sloping-bottom mode*, enabling the consistent treatment of the boundary condition in the non-horizontal parts of the bottom; this mode was introduced by the present authors (Athanassoulis & Belibassakis 1999), in connection with the corresponding water-wave propagation problem. The reader is referred to that work for a detailed analysis of the concept, its specific significance in the satisfaction of the bottom-boundary condition, and its role in accelerating the numerical convergence of the local-mode series. Therefore, in this subsection, only an outline, along with the necessary formulae, will be presented. The local-mode series expansion is

$$\varphi_{reg}(x,z;\xi)=\varphi_{-1}(x;\xi)Z_{-1}(z;x)+\varphi_0(x;\xi)Z_0(z;x)+\sum_{n=1}^{\infty}\varphi_n(x;\xi)Z_n(z;x), \tag{4.3b}$$

where $\varphi_0(x;\xi)Z_0(z;x)$ is the propagating mode, $\varphi_n(x;\xi)Z_n(z;x)$, $n=1,2,\ldots$, are the evanescent modes, and $\varphi_{-1}(x;\xi)Z_{-1}(z;x)$ is the sloping-bottom mode. The ξ-dependent functions $\varphi_n(x;\xi)$ will be called the complex *modal amplitude functions*. The function $Z_{-1}(z;x)$ is taken to satisfy: $\partial Z_{-1}(0;x)/\partial z-\mu Z_{-1}(0;x)=0$ and $\partial Z_{-1}(-h(x);x)/\partial z=1$. By the former condition, each term in the expansion (4.3*b*)

satisfies the free-surface condition individually. Thus, the representation (4.3*b*) renders the free-surface condition an essential condition in connection with the variational formulation (4.2). This proves to be very beneficial from the numerical point of view. This condition, in conjunction with the fact that $\partial Z_n(-h(x);x)/\partial z = 0$, $n = 0, 1, 2, \ldots$, leads to

$$\varphi_{-1}(x;\xi) = \frac{\partial \varphi_{reg}(x, z=-h(x);\xi)}{\partial z} \qquad \text{for any} \qquad x \in [a,b], \tag{4.4a}$$

which proves that $\varphi_{-1}(x;\xi)$ serves as a representation of the boundary values of the vertical velocity on the bottom. Note that this function cannot be non-zero on a sloping bottom, i.e. when $h'(x) \neq 0$. Also, the term $\varphi_{-1}(x;\xi)Z_{-1}(z;x)$ is not needed in the neighbourhood of the vertical interfaces $\partial D^{(12)}$ and $\partial D^{(23)}$, because both the bottom slope $h'(x)$ and the singular part of the transformed wave potential $\varphi_{sng}(\boldsymbol{x}, \boldsymbol{x}_0;\xi)$ vanish identically there. Thus, the following end conditions are imposed on the amplitude of the sloping-bottom mode, at $x = a$ and $x = b$:

$$\varphi_{-1}(a;\xi) = \varphi'_{-1}(a;\xi) = \varphi_{-1}(b;\xi) = \varphi'_{-1}(b;\xi) = 0. \tag{4.4b}$$

A suitable choice for $Z_{-1}(z;x)$ is the function

$$Z_{-1}(z;x) = h(x)[(z/h(x))^3 + (z/h(x))^2], \quad x \in [a,b], \tag{4.5}$$

although, other forms are also possible (see Athanassoulis & Belibassakis 1999, § 4).

4.3. *The coupled-mode system of horizontal equations*

Having constructed a complete local-mode (semi-discrete) representation of the function $\varphi_{reg}(x,z,\xi)$, we proceed by introducing it in the functional $\mathscr{F}_\xi$, (4.1), which now becomes a functional with arguments: the modal functions $\varphi_n(x;\xi)$, $a < x < b$, $n = -1, 0, 1, 2, \ldots$, their end-values $\varphi_n(a;\xi), \varphi_n(b;\xi)$, $n = 0, 1, 2, \ldots$, and the coefficients $C_n^{(m)}(\xi)$, $m = 1, 3$, $n = 0, 1, 2, \ldots$, defining the far-field dynamics. The variational equation (4.2) remains valid, but now the variations $\delta\varphi_{reg}$, in $D^{(2)}$, should be expressed in terms of the variations of the modal functions $\delta\varphi_n(x,\xi)$, $a < x < b$, and their end-values, $\delta\varphi_n(a;\xi)$ and $\delta\varphi_n(b;\xi)$. Furthermore, the variations $\delta(\partial\varphi^{(m)}/\partial x)$, $m = 1, 3$, on $\partial D_I^{(12)}$ and $\partial D_I^{(23)}$, should be expressed in terms of the variations $\delta C_n^{(m)}$ of the corresponding coefficients. After the necessary algebraic manipulation (cf. Athanassoulis & Belibassakis 1999, § 5), we obtain the following result:

Theorem B: *The coupled-mode system. For $\xi \in S_{c0}^+ \backslash \Xi$, the variational equation (4.2) and, thus, the matching-boundary value problem (3.17), are equivalent to the following system of second-order ordinary differential equations*:

$$\sum_{n=-1}^{\infty} \{\alpha_{mn}(x)\varphi_n''(x;\xi) + \beta_{mn}(x)\varphi_n'(x;\xi) + (\gamma_{mn}(x) - \xi^2\alpha_{mn}(x))\varphi_n(x;\xi)\} = -q_m(x;\xi), \tag{4.6a}$$

in $a < x < b$, $m = -1, 0, 1, \ldots$, supplemented by the following, homogeneous boundary conditions:

$$\varphi_{-1}(a;\xi) = \varphi'_{-1}(a;\varphi) = 0, \quad \varphi_{-1}(b;\xi) = \varphi'_{-1}(b;\xi) = 0, \tag{4.6b}$$

$$\varphi_0'(a;\xi) + \mathrm{i}\mathscr{K}_0^{(1)}(\xi)\varphi_0(a;\xi) = 0, \quad \varphi_n'(a;\xi) - \mathrm{i}\mathscr{K}_n^{(1)}(\xi)\varphi_n(a;\xi) = 0, \ n = 1, 2, \ldots, \tag{4.6c}$$

$$\varphi_0'(b;\xi) - \mathscr{K}_0^{(3)}(\xi)\varphi_0(b;\xi) = 0, \quad \varphi_n'(b;\xi) + \mathscr{K}_n^{(3)}(\xi)\varphi_n(b;\xi) = 0, \ n = 1, 2, \ldots, \tag{4.6d}$$

where a prime denotes differentiation with respect to x. The right-hand side (forcing)

	$m=-1$	$m=0,1,2,\ldots$	$m=0,1,2,\ldots$
	$n=-1,0,1,2,\ldots$	$n=-1$	$n=0,1,2,\ldots$
$\alpha_{mn}(x)$	$\langle Z_{-1}, Z_n\rangle$	$\langle Z_m, Z_{-1}\rangle$	$\delta_{mn}\|Z_m\|^2$
$\beta_{mn}(x)$	$2\langle Z_{-1}, \partial Z_n/\partial x\rangle$	$2\langle Z_m, \partial Z_{-1}/\partial x\rangle$	$2\langle Z_m, \partial Z_n/\partial x\rangle$ $+h'(x)Z_m(-h)Z_n(-h)$
$\gamma_{mn}(x)$	$\langle Z_{-1}, \nabla^2 Z_n\rangle$	$\langle Z_m, \nabla^2 Z_{-1}\rangle$ $+\left(1+h'(x)\dfrac{\partial Z_n(-h)}{\partial x}\right)Z_m(-h)$	$\langle Z_m, \nabla^2 Z_n\rangle$ $+h'(x)Z_m(-h)(\partial Z_n(-h)/\partial x)$

TABLE 1. Coefficients of the coupled-mode system, (4.6*a*). The symbols $\|\cdot\|$ and $\langle\cdot,\cdot\rangle$, respectively stand for the norm and the inner product of the space $L^2(-h(x),0)$, the integration being preformed with respect to the vertical variable $z\in[-h(x),0]$.

of the system is given by

$$q_m(x;\xi)=\int_{z=-h(x)}^{z=0} g(x,z;\xi)Z_m(z;x)\,\mathrm{d}z+f(x;\xi)Z_m(z=-h(x);x),\quad m=-1,0,1,2\ldots \tag{4.7}$$

where the function g and f have been defined by (3.16*b*, *c*, *d*) and (3.18), respectively. Also, the coefficients $\mathscr{K}_n^{(m)}(\xi)$, $n=0,1,2,\ldots,i=1,3$, appearing in the end-conditions (4.6*c*, *d*), which realize the interaction between the near-field and the far-field dynamics, are given by equations (2.8).

The coefficients $C_n^{(m)}(\xi)$, $m=1,3$, of the expansion of the wave potential in the two half-strips are then obtained by the equations:

$$C_0^{(1)}(\xi)=\varphi_0(a;\xi)\exp(a\mathscr{K}_0^{(1)}(\xi)),\quad C_n^{(1)}(\xi)=\varphi_n(a;\xi),\quad n=1,2,3,\ldots, \tag{4.8a,b}$$

$$C_0^{(3)}(\xi)=\varphi_0(b;\xi)\exp(-b\mathscr{K}_0^{(3)}(\xi)),\quad C_n^{(3)}(\xi)=\varphi_n(b;\xi),\quad n=1,2,3,\ldots. \tag{4.8c,d}$$

The coefficients $\alpha_{mn}(x)$, $\beta_{mn}(x)$ and $\gamma_{mn}(x)$, appearing in (4.6*a*), are ξ-independent functions of the horizontal variable x, obtained by means of the vertical local-modes $Z_n(z;x)$, $a\leqslant x\leqslant b$, as indicated in table 1. Since $Z_n(z;x)$ are dependent on the depth function $h(x)$, the smoothness of $\alpha_{mn}(x)$, β_{mn}, $\gamma_{mn}(x)$ is controlled by the smoothness of $h(x)$. Thus, if $h(x)$ belongs to the class C^{s+2}, of $(s+2)$-times continuously differentiable functions, the coefficients $\gamma_{mn}\in C^s$, $\beta_{mn}\in C^{s+1}$ and $\alpha_{mn}\in C^{s+2}$.

4.4. *Properties of the solution of the coupled-mode system*

The coupled-mode system (4.6) is solved numerically by means of a central second-order finite-difference scheme, as will be briefly described in § 5.1. The most important property of the system (4.6) is the rapid decay of $\varphi_n(x;\xi)$ with respect to n, which makes the modal series (4.3*b*) rapidly convergent. In fact, numerical convergence is usually achieved by using in total 5 or 6 modes (terms) in the series. It can be shown theoretically that for any constant $\xi\in S_{c0}^+$, the following estimate is valid (Athanassoulis & Belibassakis 2003):

$$\max_{a\leqslant x\leqslant b}|\varphi_n(x;\xi)|=O(n^{-4}). \tag{4.9}$$

This rapid decay is the most important consequence of the presence of the sloping-bottom mode $\varphi_{-1}(x;\xi)Z_{-1}(z;x)$ in the local-mode series representation of

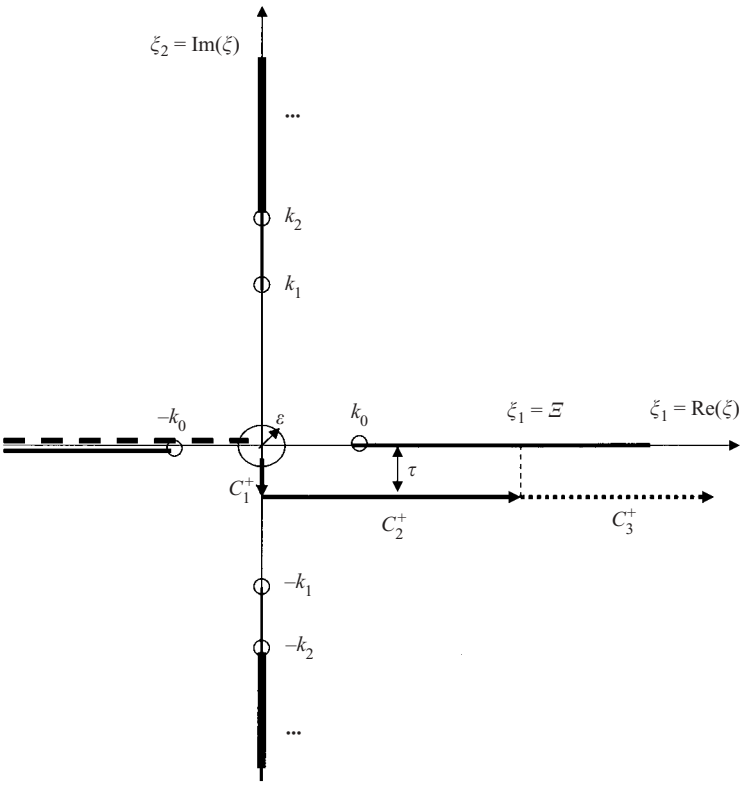

FIGURE 4. The path $(C_1^+) \cup (C_2^+) \cup (C_3^+)$ of integration on the complex ξ-domain, selected in order to facilitate numerical Fourier inversion by means of FFT.

$\varphi_{reg}(\boldsymbol{x}, \boldsymbol{x}_0; \xi)$. Without this extra term, the rate of decay of $|\varphi_n(x;\xi)|$ is only $O(n^{-2})$ (cf. Athanassoulis & Belibassakis 1999, § 6).

Clearly, the solution $\varphi_n(x;\xi), n \geqslant -1$, of the coupled-mode system (4.6), is also parametrically dependent on ξ, since the coefficients $\mathscr{K}_n^{(m)}(\xi), n \geqslant 0, m = 1, 3$, and the forcing terms $q_n(x;\xi), n \geqslant -1$, are ξ-dependent. On the basis of generic mathematical results (see e.g. Gohberg & Krein 1969, Chap. 1, § 5), it is expected that $\varphi_n(x;\xi), n \geqslant -1$, will be ξ-analytic in the common domain of ξ-analyticity of $\mathscr{K}_n^{(m)}(\xi)$ and $q_n(x;\xi)$, with the possible exception of certain isolated points, corresponding to non-trivial solutions of the homogeneous version of problem (2.5). Note that such exceptional points cannot exist for bottom profiles $h(x)$, for which a uniqueness proof is available. See e.g. Vainberg & Maz'ja (1973).

As discussed in § 3.2, $\mathscr{K}_n^{(m)}(\xi)$ are analytic functions of ξ in the half-strip S_{c0}^+. Moreover, the forcing terms $q_n(x;\xi), n \geqslant -1$, being defined by means of the functions $g(\boldsymbol{x}, \boldsymbol{x}_0; \xi)$ and $f(x, \boldsymbol{x}_0; \xi)$, (3.16) and (3.18), that involve the Bessel-functions $K_0(\xi|\boldsymbol{x} - \boldsymbol{x}_0|)$, $K_0(\xi x_F)$ and $\xi K_1(\xi x_F)$, will exhibit a branch-point (integrable) singularity at $\xi = 0$. We select the associated branch cut to be directed along the negative real axis, as shown in figure 4 by a dashed line. On the basis of the above, for the cases of the bathymetries ensuring uniqueness, the solution $\varphi_n(x;\xi), n \geqslant -1$, of the coupled-mode system is expected to be analytic for $\xi \in S_{c0}^+ \backslash \{0\}$. All the above observations concerning the ξ-analyticity remain valid for $\varphi_{reg}(\boldsymbol{x}, \boldsymbol{x}_0; \xi)$, since the latter is obtained as a uniformly convergent series of analytic functions, see e.g. Markushevich (1965, Chap. 15, § 75).

Since $\varphi_{reg}(\boldsymbol{x}, \boldsymbol{x}_0; \xi)$ will be Fourier inverted in order to obtain the solution of the three-dimensional problem, it is important to know its behaviour as $\xi_1 \to \infty, \xi = \xi_1 + \mathrm{i}\xi_2 \in S_{c0}^+$. To this end, we examine first the asymptotic behaviour of all ξ-dependent terms appearing in the system (4.6). All the forcing terms $q_n(x;\xi), n \geqslant -1$, exhibit an exponential decay

$$|q_n(x;\xi)| \leqslant Q_n^{\alpha} \xi^p \exp\big(-\xi Q_n^{\beta}\big), \tag{4.10}$$

where $p = \pm 1/2$ and $Q_n^{\alpha}, Q_n^{\beta}, n = -1, 0, 1, 2 \ldots$, are positive constants. This result stems from the corresponding behaviour of the Bessel functions $K_0(\xi|\boldsymbol{x}-\boldsymbol{x}_0|)$, $K_0(\xi x_F)$ and $\xi K_1(\xi x_F)$ involved in the definition of $q_n(x;\xi)$. Moreover, for $\xi_1 \to \infty, \xi \in S_{c0}^+$, the coefficients $\mathscr{K}_0^{(m)}(\xi) \approx \mathrm{i}\xi$ and $\mathscr{K}_n^{(m)}(\xi) \approx \xi, n \geqslant 1, m = 1, 3$.

Invoking standard WKB theory, see e.g. Bender & Orszag (1978), we seek an approximation of the solution to the coupled-mode system (4.6) in the form

$$\varphi_n(x;\xi) = \psi_n(x;\xi) \exp(-\xi S_n(x)), \quad n \geqslant -1, \tag{4.11a}$$

where $\psi_n(x;\xi)$ are assumed to be slowly varying, ξ-bounded functions and $S_n(x)$ is a ξ-independent function, controlling the phase of the corresponding modes $\varphi_n(x;\xi)$. Using (4.11*a*) in the differential equations, we obtain at the leading-order $O(\xi^2)$ of approximation the 'eikonal' equation,

$$(S_n'(x))^2 = 1 \Rightarrow S_n(x) = \pm(x - x_0), \quad n \geqslant -1. \tag{4.11b}$$

Using (4.11) in the boundary conditions of the coupled-mode system, which for large $\xi = \xi_1 + \mathrm{i}\xi_2 \in S_{c0}^+ (\xi_1 \to \infty)$ become asymptotically

$$\varphi_n'(a) - \xi\varphi_n(a) = 0 \quad \text{and} \quad \varphi_n'(b) + \xi\varphi_n(b) = 0, \quad n \geqslant -1, \tag{4.12}$$

we obtain the following result concerning the asymptotic behaviour of the solution (for $x \neq x_0$):

$$|\varphi_n(x;\xi)| \leqslant \Psi_n \exp(-\xi|x - x_0|), \quad n \geqslant -1, \tag{4.13}$$

where $\Psi_n, n = -1, 0, 1, 2 \ldots$, are positive constants. Thus, $\varphi_{reg}(\boldsymbol{x}, \boldsymbol{x}_0; \xi)$, being a linear superposition of $\varphi_n(x;\xi), n \geqslant -1$, with ξ-independent coefficients, is also expected to be analytic for $\xi \in S_{c0}^+ \backslash \{0\}$, exhibiting the asymptotic behaviour

$$|\varphi_{reg}(\boldsymbol{x}, \boldsymbol{x}_0; \xi)| \leqslant \Psi \exp(-\xi|x - x_0|) \quad \text{as} \quad \xi_1 \to \infty, \quad \xi = \xi_1 + \mathrm{i}\xi_2 \in S_{c0}^+, \tag{4.14}$$

where ψ is a positive constant (depending on $\boldsymbol{x}$ and $\boldsymbol{x}_0$).

5. Numerical solution of the three-dimensional problem

In this section, the discrete scheme used for the solution of the three-dimensional problem $\mathscr{P}_{3D}(D_{3D}, \mu, \boldsymbol{r}_0)$, equations (2.3), is briefly described. This consists of the following steps: First, the coupled-mode system of differential equations (4.6) is solved, after truncation, by using a finite-difference scheme. The system is solved for a large number of values of the Fourier parameter ξ, of the form $\xi = \xi_1 - \mathrm{i}\tau$, with $0 < \xi_1 < \Xi$, where $\Xi > 0$ is appropriately large, and $\tau > 0$, an appropriately small number. This solution, in conjunction with the local-mode representation (4.3) in $D^{(2)}$ and the representations (2.7) in the two half-strips, enables us to calculate the regular part of the transformed wave potential $\varphi_{reg}(\boldsymbol{x}, \boldsymbol{x}_0; \xi)$ throughout the whole two-dimensional domain D. The last, but not trivial, step is to carry out the Fourier inversion, (2.4*b*) or (2.14). This task concerns only $\varphi_{reg}(\boldsymbol{x}, \boldsymbol{x}_0; \xi)$, since, as already mentioned in § 3, the singular $\varphi_{sng}(\boldsymbol{x}, \boldsymbol{x}_0; \xi)$ has been inverted analytically; see (3.15).

5.1. *Discrete approximation of the coupled-mode system of equations*

All numerical results are based on the choice (4.5) for $Z_{-1}(z;x)$. Truncating the local-mode series (4.3) to a finite number of terms (modes), and denoting by N_e the number of evanescent modes retained, the following approximation of the regular part of the wave potential in $D^{(2)}$ is obtained:

$$\varphi_{reg}(x,z;\xi)=\sum_{n=-1}^{N_e}\varphi_n(x;\xi)Z_n(z;x),\qquad \boldsymbol{x}=(x,z).$$

The construction of the discrete system is completed by using central, second-order finite differences to approximate the derivatives in the coupled-mode system (4.6). Discrete boundary conditions are obtained by combining (4.6*a*) and (4.6*b*, *c*, *d*) and then using central differences to approximate derivatives. Thus, the discrete scheme is uniformly of second order, quite similar to the one described in Athanassoulis & Belibassakis (1999). On the basis of the above considerations, the coupled-mode system of differential equations is finally reduced to a linear algebraic system. The coefficient matrix of the system has dimension $N_d=(N_e+2)(N+1)$, where N is the number of segments subdividing the interval $[a,b]$, and consists of $(N_e+2)^2$ submatrices, each being three-diagonal. In all examples presented in this work a small number of modes ($N_e=5$) has been proved enough to obtain convergent numerical results, even for large bottom slopes. This is a consequence of the very fast rate of decay of the modal amplitude functions $|\varphi_n|=O(n^{-4})$, which was discussed earlier.

5.2. *Selection of the integration path to facilitate numerical Fourier inversion*

The regular part of the wave potential $\varphi_{reg}(\boldsymbol{x},\boldsymbol{x}_0;\xi)$ is expected to be analytic for $\xi\in S_{c0}^{+}\backslash\{0\}$, and to satisfy the bounds (4.14). In order that the solution of the problem $\mathscr{P}_{3D}(D_{3D},\mu,\boldsymbol{r}_0)$, as obtained by (4.3), (3.2) and (2.14), satisfies the radiation condition at infinity, (2.3*d*), the integration path in the inverse Fourier integral has to be indented below the positive real ξ-axis, taking care to circumvent the branch-type singularity located at $\xi=0$, e.g. by means of a small circular arc of radius ε, as schematically shown in figure 4. The same integration path has already been used by other authors in works treating similar problems in water waves and hydroacoustics; see e.g. Guo (1987), Frisk (1994).

The contour of integration associated with the inverse Fourier transform (2.14) can be deformed into a new path (C^{+}), lying within $S_{c0}^{+}\backslash\{0\}$. A possible choice is the path $(C_1^{+}(\varepsilon))\cup(C_2^{+})\cup(C_3^{+})$, as shown in figure 4. This path is composed of the parts: $(C_1^{+}(\varepsilon))=\{\xi_1=0,\,-\tau<\xi_2<-\varepsilon\}$, $(C_2^{+})=\{0<\xi_1<\Xi,\,\xi_2=-\tau\}$ and $(C_3^{+})=\{\Xi<\xi_1<\infty,\,\xi_2=-\tau\}$, where $\tau>\varepsilon>0$ are small positive numbers. Thus, the Fourier integral (2.14) can be equivalently put in the form

$$\begin{aligned}\Phi_{reg}(\boldsymbol{r},\boldsymbol{r}_0;\mu)&=2\lim_{\varepsilon\to0}\int_{(C_1^{+}(\varepsilon))\cup(C_2^{+})\cup(C_3^{+})}\varphi_{reg}(\boldsymbol{x},\boldsymbol{x}_0;\xi)\cos(\xi y)\,\mathrm{d}\xi\\&=2\lim_{\varepsilon\to0}\int_{\xi_2=-\varepsilon}^{\xi_2=-\tau}\varphi_{reg}(\boldsymbol{x},\boldsymbol{x}_0;\mathrm{i}\xi_2)\cosh(\xi_2 y)\,\mathrm{d}\xi_2+2\int_{\xi_1=0}^{\Xi}\varphi_{reg}(\boldsymbol{x},\boldsymbol{x}_0;\xi)\cos((\xi_1-\mathrm{i}\tau)y)\,\mathrm{d}\xi_1\\&\quad+2\int_{\xi_1=\Xi}^{\infty}\varphi_{reg}(\boldsymbol{x},\boldsymbol{x}_0;\xi)\cos((\xi_1-\mathrm{i}\tau)y)\,\mathrm{d}\xi_1.\end{aligned}\tag{5.1}$$

The second integral on the right-hand side of (5.1) can be expressed by using the exponential Fourier kernel, resulting in

$$\begin{aligned}\Phi_{reg}(\boldsymbol{r}, \boldsymbol{r}_0; \mu) = 2 &\int_{\xi_2=0-}^{\xi_2=-\tau} \varphi_{reg}(\boldsymbol{x}, \boldsymbol{x}_0; \mathrm{i}\xi_2) \cosh(\xi_2 y)\, \mathrm{d}\xi_2 \\ &+ \exp(\tau y) \int_{\xi_1=-\Xi}^{\Xi} \varphi_{reg}(\boldsymbol{x}, \boldsymbol{x}_0; |\xi_1| - \mathrm{i}\tau) \exp(\mathrm{i}\xi_1 y)\, \mathrm{d}\xi_1 \\ &- 2\sinh(\tau y) \int_{\xi_1=0}^{\Xi} \varphi_{reg}(\boldsymbol{x}, \boldsymbol{x}_0; \xi_1 - \mathrm{i}\tau) \exp(-\mathrm{i}\xi_1 y)\, \mathrm{d}\xi_1 \\ &+ 2 \int_{\xi_1=\Xi}^{\infty} \varphi_{reg}(\boldsymbol{x}, \boldsymbol{x}_0; \xi) \cos((\xi_1 - \mathrm{i}\tau) y)\, \mathrm{d}\xi_1, \end{aligned} \tag{5.2a}$$

where the second and the third terms on the right-hand side of (5.2*a*), considered together, are equivalent to the integral along (C_2^+). If $\tau > 0$ is an appreciably small number, then the first and the third integrals can be disregarded, without significant loss in accuracy. On the other hand, exploiting the exponential decay of the transformed wave potential $\varphi_{reg}(\boldsymbol{x}, \boldsymbol{x}_0; \xi)$, equation (4.14), the contribution of the fourth integral on the right-hand side of (5.2*a*) can also be ignored, if $\Xi > 0$ is an appropriately large positive number. Thus, we obtain the following approximation:

$$\Phi_{reg}(\boldsymbol{r}, \boldsymbol{r}_0; \mu) \approx \exp(\tau y) \int_{\xi=-\Xi}^{\Xi} \varphi_{reg}(\boldsymbol{x}, \boldsymbol{x}_0; |\xi| - \mathrm{i}\tau) \exp(\mathrm{i}\xi y)\, \mathrm{d}\xi, \quad \tau > 0, \quad \Xi > 0, \tag{5.2b}$$

which is valid for $y \leqslant 0$. The values of $\Phi_{reg}(\boldsymbol{r}, \boldsymbol{r}_0)$ for $y > 0$ are obtained by symmetry. Numerical experience has shown that it is not difficult to find regions of (small) τ and (large) Ξ values leading to $\Phi_{reg}(\boldsymbol{r}, \boldsymbol{r}_0)$ values, essentially independent of τ and Ξ (regions of numerical convergence). This is also discussed in the next subsection.

5.3. *Effective inversion by application of the fast Fourier transform*

Noticing that, for any $x \in R$ and depth z fixed, the Fourier integral (5.2*b*) has to be calculated for many transverse positions (y), this integral can be very efficiently calculated by means of the fast Fourier transform; see e.g. Elliot & Rao (1982). A similar approach has served as the basis of spectral or wavenumber integration techniques (known also as fast field programs in underwater acoustics, developed for calculating the acoustic field generated by a point source; see e.g. Di Napoli & Deavenport (1980), Jensen *et al.* (1994).

Consider the discretization of the ξ_1-interval $[0, \Xi]$, in the Fourier parameter space, into N_F equal-length segments, with endpoints

$$\xi_\ell = (\ell - 1)\Delta\xi, \quad \ell = 1, \ldots N_F + 1, \quad \text{where} \quad \Delta\xi = \frac{\Xi}{N_F}, \tag{5.3}$$

and the discretization of the y-interval $[0, Y]$, in the physical space, into the same number of equal-length segments Δy, with endpoints

$$y_j = (j - 1)\Delta y, \quad j = 1, ..N_F + 1, \quad \text{where } \Delta y = \frac{\pi}{\Delta\xi N_F} \quad \text{and} \quad Y = N_F \Delta y = \pi/\Delta\xi. \tag{5.4}$$

Moreover, the N_F-vector $\{\varphi_\ell = \varphi_{reg}(\xi_\ell - \mathrm{i}\tau), \ell = 1, \ldots N + 1\}$ is evenly extended to a $2N_F$-vector by setting

$$\varphi_\ell = \varphi_\ell, \quad \ell = 1, \ldots . N_F + 1 \quad \text{and} \quad \varphi_{2N-\ell+2} = \varphi_\ell, \quad \ell = 2, 3, \ldots . N_F. \tag{5.5}$$

On the basis of the above subdivisions and considerations, the integration (5.2*b*) over the finite interval $\xi \in [-\Xi, \Xi]$, is written in the following discrete form:

$$\frac{\Phi_{reg}(y_j)}{\exp(\tau y_j)} \approx \Delta\xi \left\{ \sum_{\ell=1}^{2N_F} \varphi_\ell \exp\left[\mathrm{i} \frac{2\pi(\ell-1)(j-1)}{2N_F} \right] \right\}, \quad j = 1, \ldots . N_F + 1. \tag{5.6}$$

The summation in (5.6) can be very efficiently performed, at once for all $y = y_j$, $j = 1, \ldots N_F + 1$, by applying the fast Fourier transform (FFT) to the array $\{\varphi_\ell, \ell = 1, 2N_F\}$, if N_F is selected to be a power of 2. The problem with the application of FFT (and of discrete Fourier transforms (DFT), in general) is that undersampling in the parametric ξ-domain causes aliasing in the physical y-domain, due to the implicit periodicity assumed by the discrete Fourier transform. In fact, the evaluation of the right-hand side (5.6) does not yield the values of the function $\Phi_{reg}(x, y_j, z, \boldsymbol{r}_0; \mu)/\exp(\tau y_j)$, at the points $y = y_j$, $j = 1, \ldots N_F + 1$, but rather

$$\sum_{n=-\infty}^{\infty} \frac{\Phi_{reg}(x, y_j + 2nY, z, \boldsymbol{r}_0; \mu)}{\exp(\tau(y_j + 2nY))};$$

see, e.g. Geckinkli & Yavuz (1983). Taking this into account, we obtain from (5.6)

$$\Phi_{reg}(x, y_j, z, \boldsymbol{r}_0; \mu) \approx \Delta\xi \exp(\tau y_j) \sum_{\ell=1}^{2N_F} \varphi_\ell \exp\left[\mathrm{i} \frac{2\pi(\ell-1)(j-1)}{2N} \right] - \sum_{\substack{n=-\infty \\ n \neq 0}}^{\infty} \Phi_{reg}(x, y_j + 2nY, z, \boldsymbol{r}_0; \mu) \exp(-2\tau n Y), \quad j = 1, \ldots N_F + 1. \tag{5.7}$$

The aliasing effect from (physical) ranges $|y| > Y$ is included in the second sum of the right-hand side of (5.7). It is clear from this equation that by moving the integration contour into the complex domain, i.e. for $\tau > 0$, the aliasing effect will be attenuated at least by a factor $\exp(-2\tau Y)$. On the other hand, τ cannot be large, since the approximation (5.2) is derived on the basis that the first and third integrals of (5.1) can be dropped, which is possible only for appreciably small values of τ. In all applications examined a value of $\Xi \approx 4$–$6 \max(k_0(x), x \in [a, b])$ is proved large enough to disregard the contribution from the integral along the contour (C_3^+). In all examples that will be presented later on, we have used a sampling of the interval $[-\Xi, \Xi]$ by $2N_F = 2^{10} = 1024$ points, and a shifting of the integration contour in S_{c0}^+ by $\tau \approx \Delta\xi$. This choice results in an elimination of the aliasing effect by a factor at least 0.002, and has been proved sufficient to disregard the contributions of the first and third integrals in the right-hand side of (5.2) without loss of numerical accuracy.

5.4. *A test case: application of the numerical procedure to a constant-depth strip*

In order to test the efficiency of the numerical techniques adopted and to justify the selection of various parameters, the whole numerical procedure described above has been applied to the well-known constant-depth Green's function, for which an analytical solution is available (John 1950). This solution can be expressed as a normal-mode series expansion of the form

$$\Phi_{an}(\boldsymbol{r}, \boldsymbol{r}_0) = \frac{\mathrm{i}}{2} \frac{k_0^2 - \mu^2}{h(k_0^2 - \mu^2) + \mu} H_0^{(1)}(k_0\rho) \cosh(k_0(z+h)) \cosh(k_0(z_0+h)) + \frac{1}{2} \sum_{n=1}^{\infty} \frac{k_n^2 + \mu^2}{h(k_n^2 + \mu^2) - \mu} K_0(k_0\rho) \cos(k_n(z+h)) \cos(k_n(z_0+h)). \tag{5.8}$$

See also Mei (1983 or 1994, Chap. 7). The above expression gives us the possibility of comparing $\Phi_{reg}(\boldsymbol{r}, \boldsymbol{r}_0)$, as obtained by numerically solving the coupled-mode system (4.6) and applying the FFT inversion scheme (5.7), with $\Phi_{reg,an}(\boldsymbol{r}, \boldsymbol{r}_0)$, defined as

$$\Phi_{reg,an}(\boldsymbol{r}, \boldsymbol{r}_0) = \Phi_{an}(\boldsymbol{r}, \boldsymbol{r}_0) - \Phi_{sng}(\boldsymbol{r}, \boldsymbol{r}_0), \tag{5.9}$$

where $\Phi_{an}(\boldsymbol{r}, \boldsymbol{r}_0)$ is given by (5.8), and $\Phi_{sng}(\boldsymbol{r}, \boldsymbol{r}_0)$ has been defined by (3.15*a*).

Similar comparisons can also be made in the Fourier domain. This becomes possible by using the Fourier transform of (5.8), which is available in analytic (normal-mode series) form, see e.g. Evans (1972),

$$\begin{aligned}\varphi_{an}(\boldsymbol{x}, \boldsymbol{x}_0; \xi) &= \frac{\mathrm{i}}{2\pi} \frac{k_0^2 - \mu^2}{h(k_0^2 - \mu^2) + \mu} \frac{\exp\left(\mathrm{i}|x - x_0|\sqrt{k_0^2 - \xi^2}\right)}{\sqrt{k_0^2 - \xi^2}} \cosh(k_0(z + h)) \cosh(k_0(z_0 + h)) \\ &+ \frac{1}{2\pi} \sum_{n=1}^{\infty} \frac{k_n^2 + \mu^2}{h(k_n^2 + \mu^2) - \mu} \frac{\exp\left(-|x - x_0|\sqrt{k_n^2 + \xi^2}\right)}{\sqrt{k_n^2 + \xi^2}} \cos(k_n(z + h)) \cos(k_n(z_0 + h)).\end{aligned} \tag{5.10}$$

Again, a comparison can be made for the regular part $\varphi_{reg}(\boldsymbol{x}, \boldsymbol{x}_0; \xi)$, for which the analytical expression

$$\varphi_{reg,an}(\boldsymbol{x}, \boldsymbol{x}_0; \xi) = \varphi_{an}(\boldsymbol{x}, \boldsymbol{x}_0; \xi) - \varphi_{sng}(\boldsymbol{x}, \boldsymbol{x}_0; \xi) \tag{5.11}$$

is available. In (5.11) $\varphi_{sng}(\boldsymbol{x}, \boldsymbol{x}_0; \xi)$ is defined by (3.11).

The above equations have been systematically used for comparisons, in order to calibrate and optimize the present numerical scheme and, especially, for assessing optimum values of the numerical parameters τ and ξ, as well as of the parameters controlling the filter function ω.

Some illustrative examples demonstrating the accuracy of the present numerical scheme are shown in figures 5 and 6. The physical parameters of the presented case are: constant depth $h = 4\,\mathrm{m}$, source frequency $\omega = 2\,\mathrm{rad\,s^{-1}}$, wavelength $\lambda = 14.5\,\mathrm{m}$, and thus, $h/\lambda = 0.27$, which corresponds to intermediate water depth. The source position is $x_0 = 10\,\mathrm{m}$ and $z_0 = -1\,\mathrm{m}$, and the end points of the intermediate domain $D^{(2)}$ have been selected to be $x = a = 0$ and $x = b = 20\,\mathrm{m}$.

The effect of shifting the contour of integration into the complex domain on the calculated wave field $\Phi(\boldsymbol{r}, \boldsymbol{r}_0)$ on the free surface ($z = 0$) is presented in figure 5. The values of the wave potential $\Phi(x, y, z = 0)$, at $y = 0$ and at $y = 100\,\mathrm{m}$, are plotted against the analytical solution $\Phi_{an}(\boldsymbol{r}, \boldsymbol{r}_0)$, equation (5.8). Numerical results, as obtained by the present method, are plotted for $\tau = 0$ (dashed lines) and $\tau = 0.01$ (solid lines). The analytical solution is denoted by dots. For $\tau = 0$, the aliasing effect contaminates the numerical solution, and this effect becomes worse as the distance of the field point from the source increases. This problem is completely remedied by moving the integration contour into the complex domain (using $\tau = 0.01$).

The effects of the filter shape and length on the numerical solution are examined in figure 6. In this figure, the real part of the functions $\Phi_{sng}(x, y, z = 0)$, $\Phi_{reg}(x, y, z = 0)$ and of their superposition $\Phi(x, y, z = 0)$, at $y = 0$, are plotted, as calculated by the present method, by using the polynomial filter (3.14*b*) with $\varepsilon = 4\,\mathrm{m}$ and $\varepsilon = 8\,\mathrm{m}$, and by using the exponential filter (3.14*a*) with filter length $\varepsilon = 8\,\mathrm{m}$. The corresponding analytical solution $\Phi_{an}(\boldsymbol{r}, \boldsymbol{r}_0)$ is denoted by dots. It is clearly seen in this figure that the solution $\Phi(\boldsymbol{r}, \boldsymbol{r}_0) = \Phi_{sng}(\boldsymbol{r}, \boldsymbol{r}_0) + \Phi_{reg}(\boldsymbol{r}, \boldsymbol{r}_0)$ remains practically unaffected by the filter

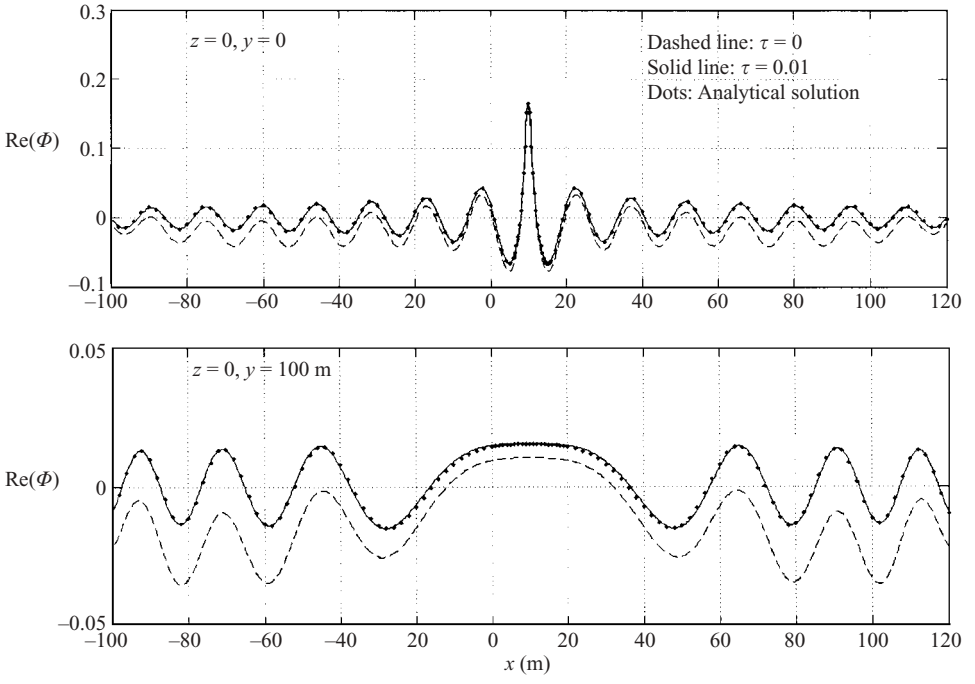

FIGURE 5. The effect of τ on the calculated wave potential Φ on the free surface, in comparison with the analytical solution (John, 1950).

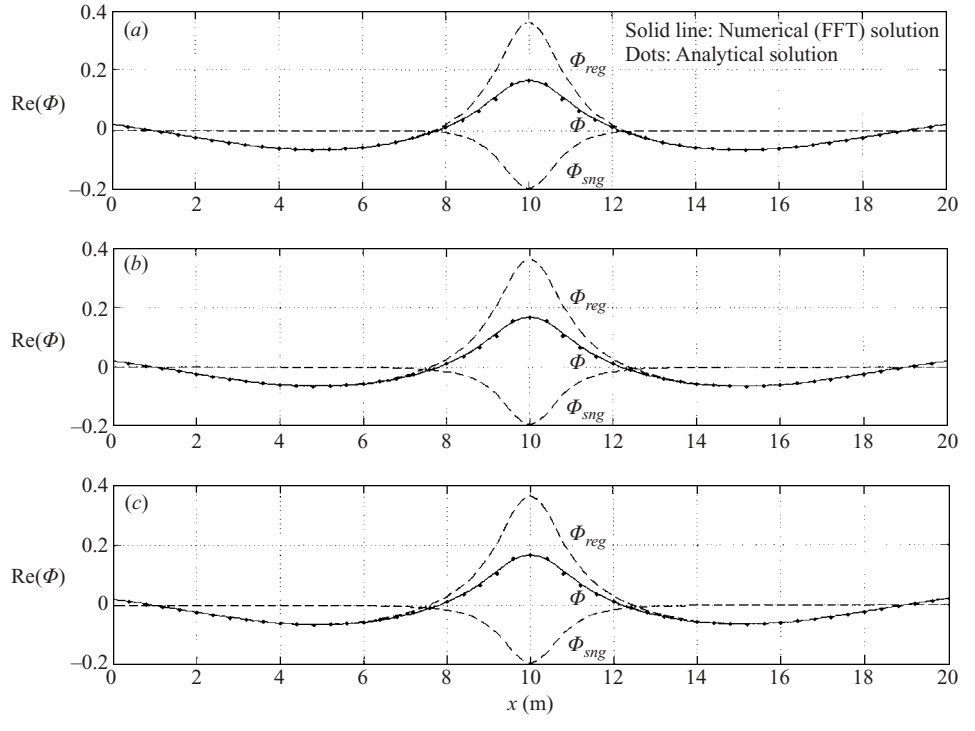

FIGURE 6. The effect of filter shape and length on the calculated wave potential Φ on the free surface at $z = 0$, $y = 0$, in comparison with the analytical solution (John, 1950): (*a*) polynomial filter, $\varepsilon = 4$ m; (*b*) polynomial filter, $\varepsilon = 8$ m; (*c*) exponential filter, $\varepsilon = 8$ m.

shape and length, always coinciding with the analytical one $\Phi_{an}(\boldsymbol{r}, \boldsymbol{r}_0)$. Changes in the filter shape and length result in slight modifications of $\Phi_{sng}(\boldsymbol{r}, \boldsymbol{r}_0)$ and $\Phi_{reg}(\boldsymbol{r}, \boldsymbol{r}_0)$, which are cancelled out by their superposition in obtaining the total wave potential.

6. Applications to various uneven bottom profiles and discussion

In this section, applications of our method to various uneven bottom profiles are presented and discussed, focusing on the identification of the important features of the near- and far-field wave patterns.

6.1. *The case of a smooth underwater shoal*

This topography has been considered by Athanassoulis & Belibassakis (1999) in order to examine the effects of bottom slope and curvature on the solution of the propagation/transmission problem obtained by the consistent coupled-mode model. It is characterized by the depth function

$$h(x) = \begin{cases} h_1 = 6\,\mathrm{m} & x < a = 0, \\ \dfrac{h_1 + h_3}{2} - \dfrac{h_1 - h_3}{2} \tanh\left(3\pi\left(\dfrac{x}{b} - \dfrac{1}{2}\right)\right), & a < x < b, \\ h_3 = 2\,\mathrm{m}, & x > b = 20\,\mathrm{m}, \end{cases} \tag{6.1}$$

which models a smooth but steep underwater shoaling, with maximum slope $s_{max} = 0.94$ and mean slope $s_{mean} = 0.2$. (A sketch of the bottom geometry is shown in figure 8 below). The source is located at $x_0 = 10\,\mathrm{m}$, $z_0 = -1\,\mathrm{m}$, and its angular frequency is taken to be $\omega = 2\,\mathrm{rad\,s^{-1}}$, implying that ratios $h_1/\lambda_1 = 0.4$ and $h_3/\lambda_3 = 0.17$ (where $\lambda_m = 2\pi/k_0^{(m)}$, $m = 1, 3$) fall outside the limits of deep- and shallow-water theory.

For the bottom profile (6.1), the horizontal structure of the real part of the wave potential (and also of the free-surface elevation η, since $\eta = \mathrm{i}\omega\Phi/g$, is shown in figure 7. From this figure we observe that a shadow zone is formed above the bottom shoaling ($0 < x < 20\,\mathrm{m}$). As $x \to \pm\infty$, in sectors not including the variable-bathymetry region, the wave pattern approaches the standard one, corresponding to cylindrical outward propagating waves at constant depths $h_1 = 6\,\mathrm{m}$ and $h_3 = 2\,\mathrm{m}$, respectively. From a systematic examination of various bottom profiles, we can state that this is a characteristic feature of the far-field pattern of the source-generated wave field, in the case of a monotonic bottom variation. This result is compatible with the far-field structure of the Green's function of the mild-slope equation, studied by Belibassakis (2000). On the basis of the results presented in Appendix B, in the case of a monotonic bed profile, the far-field asymptotic behaviour of the present three-dimensional Green's function is

$$\Phi(\boldsymbol{r}, \boldsymbol{r}_0) = F_m(\theta) \frac{\exp\left(\mathrm{i}k_0^{(m)}\rho\right)}{\sqrt{\rho}} \frac{\cosh\left(k_0^{(m)}(z + h_m)\right)}{\cosh\left(k_0^{(m)} h_m\right)} + O\left(\rho^{-3/2}\right), \quad \boldsymbol{r} \in D^{(m)}, \quad m = 1, 3, \tag{6.2a}$$

$$\Phi(\boldsymbol{r}, \boldsymbol{r}_0) = O\left(\rho^{-3/2}\right), \qquad \boldsymbol{r} \in D^{(2)}, \tag{6.2b}$$

where $\rho = \sqrt{(x - x_0)^2 + (y - y_0)^2}$, $\theta = \tan^{-1}((y - y_0)/(x - x_0))$, and $F_m(\theta)$ denotes the far-field pattern of the source potential in $D^{(m)}$, $m = 1, 3$, which is independent of the horizontal distance ρ between the source and the field points.

In figure 8, the vertical structure of the wave potential (real and imaginary parts), in the (x,z)-plane passing through the point source $(x_0, y_0 = 0, z_0)$, along with its values on the free surface, is visualized using equipotential lines. Note that the structure of

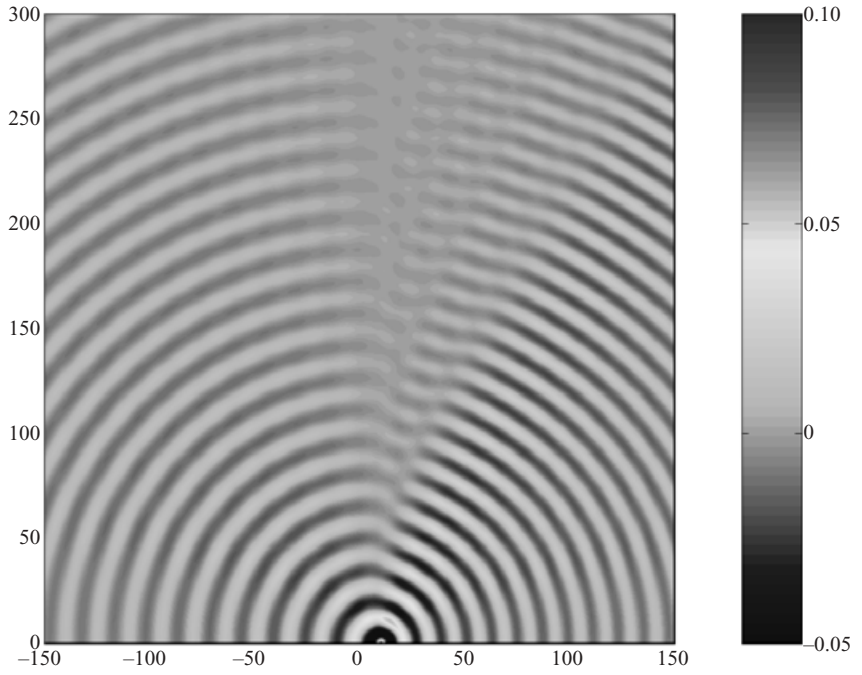

FIGURE 7. Real part of Φ on the free surface in the case of the smooth but steep upslope ($h_1 = 6\,\mathrm{m}, h_3 = 2\,\mathrm{m}$) shown in figure 8. Source frequency $\omega = 2\,\mathrm{rad\,s^{-1}}$. Source position: ($x_0 = 10\,\mathrm{m}$, $y_0 = 0$, $z_0 = -1\,\mathrm{m}$).

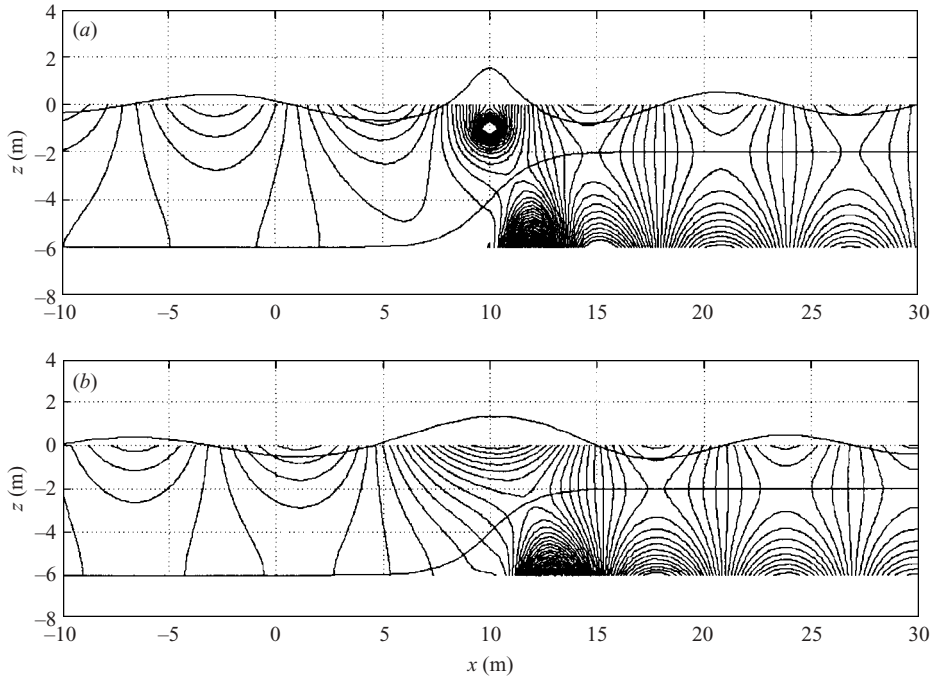

FIGURE 8. (*a*) Real and (*b*) imaginary parts of Φ on the vertical plane in the case of the smooth but steep upslope ($h_1 = 6\,\mathrm{m}, h_3 = 2\,\mathrm{m}$). Source frequency and position as in figure 7. To better illustrate the values of the wave potential on the free surface (proportional to the free-surface elevation) they have been 10 times exaggerated.

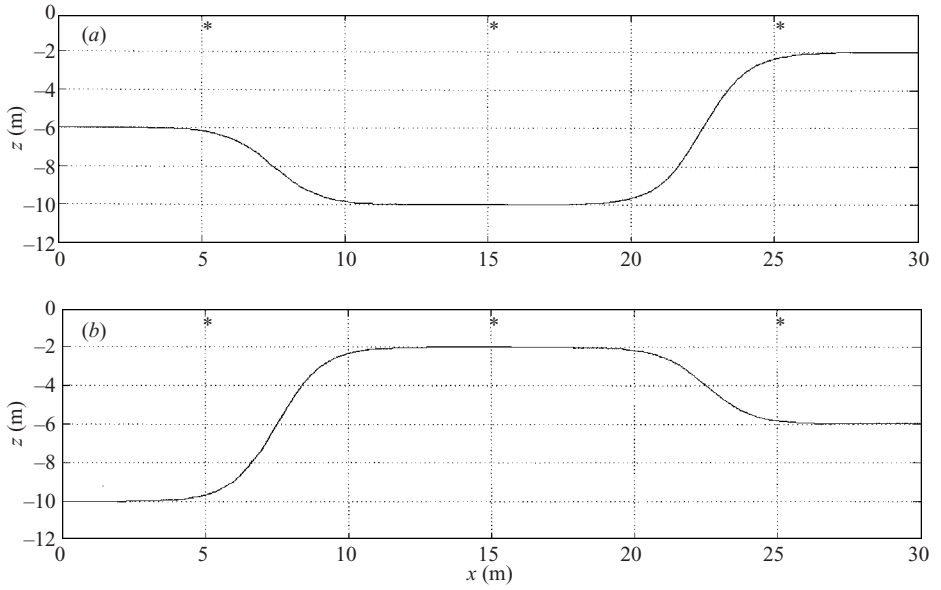

FIGURE 9. The bathymetries examined: (*a*) smooth underwater trench and (*b*) ridge. The position of the source is denoted by asterisks.

the local-mode series provides us automatically with the extension of the wave field beyond the physical boundaries. Thus, the equipotential lines have been maintained in the figure, in order to better present the fulfillment of the bottom boundary condition $\partial\Phi/\partial n = 0$, which is equivalent to orthogonality between the equipotential lines and the bottom profile. From this figure we are also able to observe the efficient representation of the point singularity, which is the result of the decomposition (3.2) and the analytical treatment of the singular part, (3.15).

To give an estimate of the computational effort required by the present method, the result corresponding to the case presented in figures 7 and 8, which is based on the calculation of the source field at the points of a grid: $x \times y \times z = 1101 \times 512 \times 41$, required 600 CPU s, using Matlab in a Pentium IV 2.4 GHz machine. For comparison, the calculation of the constant-depth Green's function (for $h = 6\,\mathrm{m}$ and the same frequency $\omega = 2\,\mathrm{rad\,s^{-1}}$), using formula (5.8) without taking into account the axial symmetry of the field, and the same number of modes, required 15 CPU s.

6.2. *Wave patterns over various non-monotonic uneven-bottom profiles*

Finally we present numerical results concerning the free-surface patterns produced by oscillating point sources over the two non-monotonic, uneven-bottom profiles shown in figure 9. The first profile models a smooth but locally very steep underwater trench, and the second profile models a smooth underwater ridge. In both cases the depths at infinity are different, and the bottom irregularity is taken to extend from $x = 0$ to $x = 30\,\mathrm{m}$. As before, the vertical position of the source is taken to be close to the free surface ($z_0 = -1\,\mathrm{m}$). The horizontal position of the source is varied, as shown in figure 9 by an asterisk ($x_0 = 5\,\mathrm{m}$, 15 m and 25 m). In all cases the source frequency is taken to be $\omega = 2\,\mathrm{rad\,s^{-1}}$, and thus, the depth-to-wavelength ratios corresponding to the characteristic depths $h = 2\,\mathrm{m}$, 6 m, 10 m of the two bottom profiles are $h/\lambda = 0.17, 0.4, 0.65$, respectively.

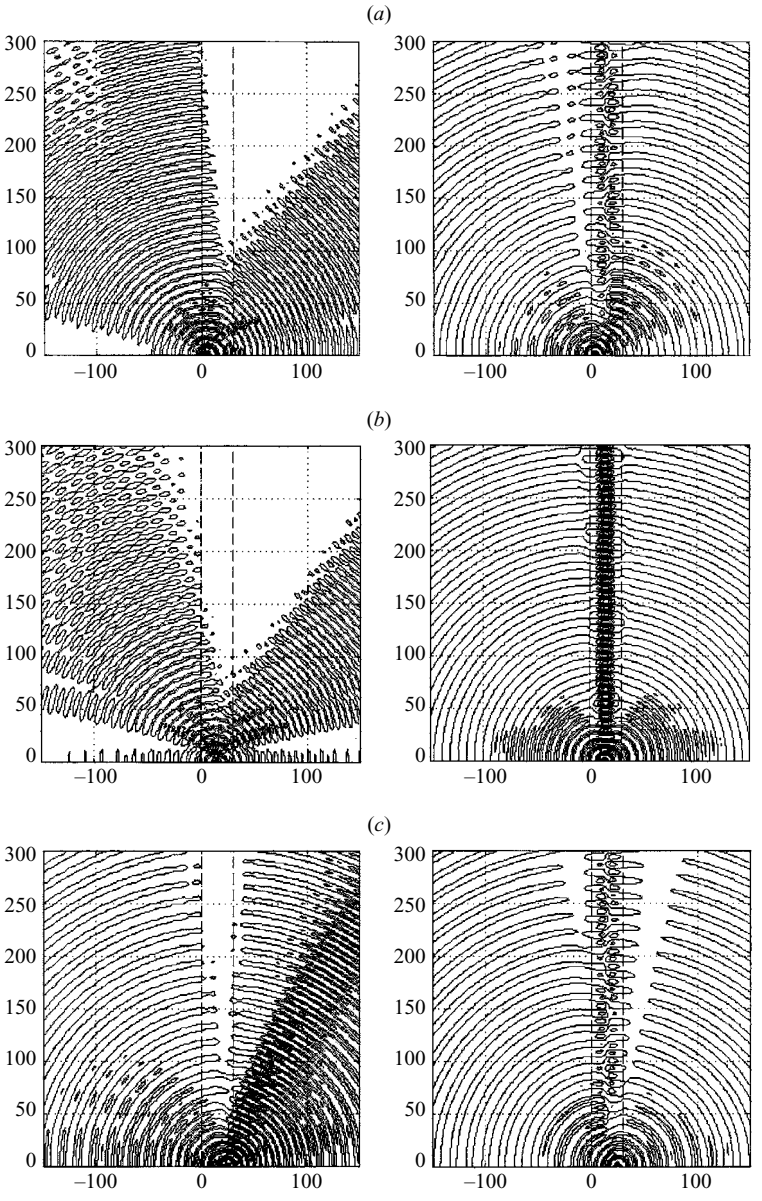

FIGURE 10. Source wave patterns on the free surface. The left-hand column corresponds to the case of the trench, and the right-hand column to the case of the ridge, shown in figure 9. In (*a*) the source is located at the left ($x_0 = 5$ m), in (*b*) at the centre ($x_0 = 15$ m), and in (*c*) at the right of the variable-bathymetry region ($x_0 = 25$ m).

The real part of the wave field on the free surface $\Phi(x, y, z = 0)$, for each of the six combinations (bottom profile–source position), is shown in figure 10, by using equipotential lines on the horizontal plane. The left-hand column of subplots corresponds to the first bottom profile (trench) and the right-hand column to the second bottom profile (ridge), respectively. Figure 10(*a*) corresponds to source positioned at $x_0 = 5$ m, 10(*b*) to $x_0 = 15$ m, and 10(*c*) to $x_0 = 25$ m. In each subplot, the

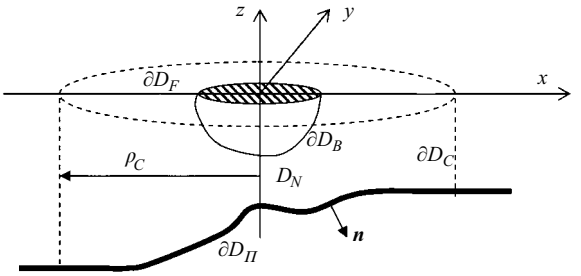

FIGURE 11. Schematic definition of the hybrid scheme.

limits of the variable-bathymetry region are shown by means of two dashed lines, at $x = 0$ and $x = 30$ m.

We observe from this figure that the free-surface field exhibits a strong azimuthal anisotropy, its fine structure being controlled by the bottom-profile geometry and the source position. More precisely, in the case of the trench (left-hand column of subplots in figure 10), the wave tends to diverge from the deep area, forming a shadow zone there. In the sectors not including the bottom irregularrity, the radiation of wave energy exhibits preferable directions, depending on the relative position of the source with respect to the trench. This is more pronounced in the case when the source is located near the right-hand end of the trench (figure 10*c*, left). Furthermore, at large distances from the source, where the depth is constant $h = h_m$, $m = 1, 3$, the wave field behaves like outgoing waves with wavelength corresponding to the sector depth, $\lambda_m = 2\pi/k_0^{(m)}$, $m = 1, 3$.

In the case of the underwater ridge (right-hand column of subplots in figure 10), the radiated energy tends to accumulate inside the limits of the ridge. If the source is located near the middle of the ridge (in the area of minimum depth), a great part of the radiated energy is trapped inside the ridge, and we observe characteristic patterns of well-localized waves, propagating parallel to the depth contours.

7. Applications to wave–body–seabed interaction problems

The Green's function developed in the present paper, which satisfies the no-entrance boundary condition on the bottom profile $z = -h(x)$, will be denoted in this section by $G(\boldsymbol{r}|\boldsymbol{r}_0)$, and the associated singularity will be called the bottom-dependent source (in short, bd-source). This Green's function has important applications to the solution of wave–body–seabed interaction problems, either directly, in the framework of boundary integral equations (see e.g. Wehausen 1974, part 4), or in the context of hybrid techniques (see e.g. Bai & Yeung 1974; Euvrard *et al.* 1981; Mei 1983). The direct use of the present bd-Green's function in boundary integral equations supported only on the wetted surface of the body would require significant computer resources, but it is desirable at least for providing high-quality benchmark solutions for testing other existing, less computationally intensive methods, which only approximately comply with the correct behaviour at infinity.

Perhaps the most promising way to exploit the present bd-source for solving complex wave–body–seabed interaction problems is in the context of some hybrid schemes. In such schemes, different representations of the solution are used in the near field D_N, which encloses the body and the variable-bathymetry region, and in the far field $D|D_N$; see figure 11. Here, the two subdomains are defined by means

of the cylindrical surface $\rho = \rho_C$, decomposing the whole liquid domain D into the interior (near-field) D_N and the exterior (far-field) $D|D_N$.

One such scheme can be formulated by using simple (Rankine) sources for the wave field in D_N,

$$\Phi(\boldsymbol{r}) = \int_{\partial D_N} \sigma_N(\boldsymbol{r}_0) G_N(\boldsymbol{r}|\boldsymbol{r}_0)\, \mathrm{d}S(\boldsymbol{r}_0), \quad \boldsymbol{r} \in D_N, \tag{7.1}$$

where G_N denotes the simple source given by (3.1), in conjunction with a representation of the wave field in $D \backslash D_N$ by means of a distribution of bd-sources on the wetted surface of the body:

$$\Phi(\boldsymbol{r}) = \int_{\partial D_B} \sigma(\boldsymbol{r}_0) G(\boldsymbol{r}|\boldsymbol{r}_0)\, \mathrm{d}S(\boldsymbol{r}_0), \quad \boldsymbol{r} \in D \backslash D_N, \tag{7.2}$$

Subdividing the wetted surface of the body, ∂D_B, in a union of sufficiently small, disjoint boundary elements $\{E_i, i = 1, I\}$, and taking the distance between the body and the cylindrical surface $\rho = \rho_C$ to be large enough (of the order of a few wavelengths), the following approximation for the wave potential in the exterior domain is easily obtained:

$$\Phi(\boldsymbol{r}) = \int_{\cup E_i} \sigma(\boldsymbol{r}_0) G(\boldsymbol{r}|\boldsymbol{r}_0)\, \mathrm{d}S(\boldsymbol{r}_0) \approx \sum_{i=1}^{I} \sigma(\boldsymbol{r}_{0,i}) G(\boldsymbol{r}|\boldsymbol{r}_{0,i}) S_i, \quad \boldsymbol{r} \in D \backslash D_N, \tag{7.3}$$

where $\boldsymbol{r}_{0,i}$ denotes the centroid of the surface panel E_i, and S_i denotes its area. Then the diffraction–refraction–radiation problems associated with the wave–body–seabed interaction can be solved by means of the following system of equations (defining the hybrid scheme):

$$-\frac{\sigma_N(\boldsymbol{r})}{2} + \int_{\partial D_N} \sigma_N(\boldsymbol{r}_0) \frac{\partial G_N(\boldsymbol{r}|r_0)}{\partial n}\, \mathrm{d}S(\boldsymbol{r}_0) = \begin{cases} g(\boldsymbol{r}), & \boldsymbol{r} \in \partial D_B \\ 0, & \boldsymbol{r} \in \partial D_\Pi, \end{cases} \tag{7.4}$$

$$-\frac{\sigma_N(\boldsymbol{r})}{2} + \int_{\partial D_N} \sigma_N(\boldsymbol{r}_0) \left(\frac{\partial G_N(\boldsymbol{r}|\boldsymbol{r}_0)}{\partial n} - \mu G_N(\boldsymbol{r}|\boldsymbol{r}_0) \right) \mathrm{d}S(\boldsymbol{r}_0) = 0, \quad \boldsymbol{r} \in \partial D_F, \tag{7.5}$$

where ∂D_F, ∂D_Π denote the free-surface and bottom-boundary parts of D_N, $\boldsymbol{n}$ is the unit normal vector directed to the exterior of D_N, and the Neumann data

$$g(\boldsymbol{r}) = -\frac{\partial \Phi_{inc}}{\partial n} \quad \text{or} \quad n_k \quad \text{or} \quad (\boldsymbol{r} \times \boldsymbol{n})_k, \quad k = 1, 2, 3, \quad \text{if} \quad \boldsymbol{r} \in \partial D_B, \tag{7.6}$$

are defined through the solution (Φ_{inc}) of the wave propagation–refraction problem over the same variable-bathymetry region, without the presence of the body (the diffraction problem), or by the components of the generalized normal vector (the radiation problems).

The formulation of the hybrid scheme is completed by the matching conditions, expressing the continuity of the potential and of its normal derivative, respectively, on the surface of the vertical cylinder ∂D_C:

$$\int_{\partial D_N} \sigma_N(\boldsymbol{r}_0) G_N(\boldsymbol{r}|\boldsymbol{r}_0)\, \mathrm{d}S(\boldsymbol{r}_0) - \sum_{i=1}^{I} \sigma(\boldsymbol{r}_{0,i}) G(\boldsymbol{r}|\boldsymbol{r}_{0,i}) S_i = 0, \quad \boldsymbol{r} \in \partial D_C, \tag{7.7a}$$

$$-\frac{\sigma_N(\boldsymbol{r})}{2} + \int_{\partial D_N} \sigma_N(\boldsymbol{r}_0) \frac{\partial G_N(\boldsymbol{r}|\boldsymbol{r}_0)}{\partial n}\, \mathrm{d}S(\boldsymbol{r}_0) - \sum_{i-1}^{I} \sigma(\boldsymbol{r}_{0,i}) \frac{\partial G(\boldsymbol{r}|\boldsymbol{r}_{0,i})}{\partial n} S_i = 0, \quad \boldsymbol{r} \in \partial D_C. \tag{7.7b}$$

In accordance with existing numerical experience, the above matching conditions should be implemented in an appropriate weak (Galerkin) form.

In conluding this subsection, we note that if ρ_C is taken to be very large ($\rho_C \to \infty$), then only one term in (7.3) is sufficient ($I = 1$), corresponding to only one bd-source (located at $\boldsymbol{r}_{0,1}$). In this case, the unique coefficient $\sigma(\boldsymbol{r}_{0,1})$ can be eliminated from (7.7), resulting in

$$-\frac{\sigma_N(\boldsymbol{r})}{2} + \int_{\partial D_N} \sigma_N(\boldsymbol{r}_0)\left(\frac{\partial G_N(\boldsymbol{r}|\boldsymbol{r}_0)}{\partial n} - \mathscr{U}(\boldsymbol{r})G_N(\boldsymbol{r}|\boldsymbol{r}_0)\right)\mathrm{d}S(\boldsymbol{r}_0) = 0, \quad \boldsymbol{r} \in \partial D_C, \quad (7.8a)$$

or

$$\frac{\partial \Phi(\boldsymbol{r})}{\partial n} - \mathscr{U}(\boldsymbol{r})\Phi(\boldsymbol{r}) = 0, \quad \boldsymbol{r} \in \partial D_C, \quad (7.8b)$$

where the function $\mathscr{U}(\boldsymbol{r})$ is defined as the ratio

$$\mathscr{U}(\boldsymbol{r}) = \frac{1}{G(\boldsymbol{r}|\boldsymbol{r}_{0,1})}\frac{\partial G(\boldsymbol{r}|\boldsymbol{r}_{0,1})}{\partial n}, \quad \boldsymbol{r} \in \partial D_C. \quad (7.8c)$$

The last result can be considered as a generalization of the classical Sommerfeld radiation condition in the presence of an uneven bottom profile. Ideas and techniques for the hydrodynamic analysis of floating and/or immersed bodies in variable-bathymetry regions, initiated in this section, will be presented in more detail, along with numerical results, elsewhere (Belibassakis 2004).

8. Concluding remarks

In the present work, the three-dimensional Green's function of harmonic water waves, in variable-bathymetry regions with different depths at infinity in different directions (bd-Green's function), is derived and studied. The concept of this approach and initial results have been presented by the present authors in Athanassoulis & Belibassakis (1997). In addition to its intrinsic interest, the bd-Green's function provides useful information for the formulation and treatment of complex wave–body–seabed interaction problems in variable-bathymetry regions, supporting the hydrodynamic analysis of large structures in the nearshore and coastal environment.

The fact that the depth is not uniform at infinity introduces a strong azimuthal anisotropy there, and makes the problem unusual, in the sense that the far-field behaviour is not known *a priori* and, thus, it should be found as part of the solution. The problem is treated by using Fourier transform, reducing it to a two-dimensional boundary value problem on the vertical plane, governed by the modified Helmholtz equation with Fourier parameter ξ, and the usual free-surface and bottom boundary conditions. The two-dimensional problem is solved by an appropriate extension of the consistent coupled-mode method developed by Athanassoulis & Belibassakis (1999) for water-wave propagation in variable-bathymetry regions. An essential new feature of the problem studied here is the presence of the physical-space singularity, which calls for a delicate numerical treatment in the wavenumber domain. To avoid numerical Fourier inversion of singular functions and to maintain the rapid convergence of the enhanced local-mode series, the total wave potential is appropriately decomposed into an analytically defined singular part, which fulfils the free-surface boundary condition and is Fourier-invertible in closed form, and in a regular part, which also satisfies the free-surface boundary condition and a regularly forced modified Helmholtz equation. The regular wave potential is represented by an enhanced local-mode series and, with

the aid of an appropriate variational principle, is reformulated as a forced system of horizontal differential equations for the complex modal-amplitude functions.

The coupled-mode system is numerically solved for many values of the Fourier parameter ξ, by using a second-order, central, finite-difference scheme. Then, the three-dimensional pulsating-source wave potential is obtained by an efficient numerical Fourier inversion scheme based on FFT. To eliminate the aliasing effect associated with FFT, contour integration on the complex plane is used, enabled by the appropriate extension of the transformed problem and the coupled-mode system to complex ξ. Numerical results are presented and discussed for various bottom topographies, including smooth but steep underwater trenches and ridges, putting emphasis on the identification of the important features of the near- and far-field patterns on the horizontal plane and on the vertical plane containing the point source. Characteristic patterns of trapped (well-localized) wave propagation over ridges have been predicted and discussed.

A direct application of the present work can be its exploitation for the hydrodynamic analysis of large three-dimensional structures over uneven bottom topographies, directly in the framework of the boundary integral equation methods with support only on the surface of the body(ies). Furthermore, the present Green's function can be used in order to provide a concise far-field closure condition in hybrid schemes, where the near field (in the vicinity of the structure) is treated by any other efficient solution technique, e.g. Rankine sources, FEM or spectral-type techniques.

The authors are indebted to the anonymous referees for their constructive comments and suggestions which helped them in improving some points of the presentation and motivated the additional results presented in § 7 and in the Appendices.

Appendix A. The case of a point source lying far from the bottom irregularity

In the case where the point source lies in $D^{(m)}$, $m=1$ or 3, at a great distance from the variable-bathymetry region $D^{(2)}$, we can apply a decomposition into singular and regular parts

$$\Phi(\boldsymbol{r}, \boldsymbol{r}_0) = \Phi_{sng}(\boldsymbol{r}, \boldsymbol{r}_0) + \Phi_{reg}(\boldsymbol{r}, \boldsymbol{r}_0), \tag{A 1}$$

using as singular part $\Phi_{sng}(\boldsymbol{r}, \boldsymbol{r}_0)$ the constant-depth Green's function (John 1950; see also (5.8)) formulated at the corresponding depth h_m. In this case, since $k_0\rho \gg 1$, the far-field asymptotics of $\Phi_{sng}(\boldsymbol{r}, \boldsymbol{r}_0)$ can be used for $a < x < b$,

$$\Phi_{sng}(\boldsymbol{r}, \boldsymbol{r}_0) \approx A_{sng}\sqrt{\frac{2\pi}{k_0\rho}}\exp\left(\mathrm{i}k_0\rho - \frac{\mathrm{i}\pi}{4}\right)\cosh(k_0(z+h_m)), \tag{A 2}$$

where

$$A_{sng} = \frac{\mathrm{i}}{2\pi}\frac{k_0^2-\mu^2}{h_m(k_0^2-\mu^2)+\mu}\cosh(k_0(z_0+h_m)), \tag{A 3}$$

$\rho = \sqrt{(x-x_0)^2+y^2}$, and k_0 denotes the propagating wavenumber associated with the frequency parameter μ and the corresponding depth h_m (as obtained by (2.10a)).

The function $\Phi_{sng}(\boldsymbol{r}, \boldsymbol{r}_0)$ can also be represented through its Fourier transform (see (5.10)), as follows:

$$\Phi_{sng}(\boldsymbol{r}, \boldsymbol{r}_0) = A_{sng}\cosh(k_0(z+h_m))\int_{\xi=-\infty}^{\xi=+\infty}\frac{\exp\left(\mathrm{i}\left(|x-x_0|\sqrt{k_0^2-\xi^2}+y\xi\right)\right)}{\sqrt{k_0^2-\xi^2}}\,\mathrm{d}\xi. \tag{A 4}$$

Expression (A 4) can be asymptotically ($k_0\rho \gg 1$) put in a more convenient form, by ignoring the rapidly decaying part $|\xi| > k_0$ of the integral, and introducing the transformation $\xi = k_0 \sin\theta$ that eliminates the pair of branch points at $\xi = \pm k_0$ (see e.g. Felsen & Marcuvitz 1973, § 5). In this way, the function $\Phi_{sng}(\boldsymbol{r}, \boldsymbol{r}_0)$ is asymptotically represented as the superposition of obliquely incident plane waves, propagating with angle $\theta(-\frac{1}{2}\pi < \theta < \frac{1}{2}\pi)$ with respect to the bottom contours,

$$\Phi_{sng}(\boldsymbol{r}, \boldsymbol{r}_0) \approx A_{sng} \cosh(k_0(z + h_m)) \int_{\theta=-\pi/2}^{\theta=\pi/2} \exp(\mathrm{i}k_0(|x - x_0| \cos\theta + y \sin\theta))\, \mathrm{d}\theta. \quad \text{(A 5)}$$

Thus, in the case when the point source lies in one of the two constant-depth strips away from the bottom irregularity, the solution of the present problem can be obtained in the form of a Weyl-type integral, as follows:

$$\Phi(\boldsymbol{r}, \boldsymbol{r}_0) = A_{sng} \int_{\theta=-\pi/2}^{\theta=-\pi/2} \mathscr{H}(\boldsymbol{r}; \theta) \exp(\pm \mathrm{i}k_0 x_0 \cos\theta)\, \mathrm{d}\theta, \quad \text{(A 6)}$$

where $\mathscr{H}(\boldsymbol{r}; \theta)$ denotes the complex transfer function associated with the propagation/transmission of obliquely incident plane waves, propagating at an angle θ from $D^{(m)}$ through $D^{(2)}$. This transfer function can be very efficiently calculated, for all angles of incidence θ, by application of the present coupled-mode technique, as described in Belibassakis, Athanassoulis & Gerosthathis (2001, § 3).

Appendix B. The leading-order far-field asymptotics of the point-source wave field

B.1. *The point source in* $D^{(2)}$

In the case where the point source is in $D^{(2)}$, and the field point lies in $D^{(m)}$, $m = 1$ or 3, at a great distance from the source ($x \ll a$ or $x \gg b$), our solution is obtained through (2.4*b*) by retaining only the first terms ($n = 0$) in the representations (2.7) (all other terms decay exponentially away from $x = a$ or $x = b$),

$$\Phi(\boldsymbol{r}, \boldsymbol{r}_0) = Z_0^{(m)}(z) \int_{\xi=-\infty}^{\xi=+\infty} C_0^{(m)}(\xi) \exp\left(\mathrm{i}\left(|x| \sqrt{\left(k_0^{(m)}\right)^2 - \xi^2} + y\xi\right)\right) \mathrm{d}\xi, \quad m = 1, 3, \quad \text{(B 1)}$$

where the functions $Z_0^{(m)}(z)$ are defined by (2.10*b*). Without loss of generality we shall set $a = 0$. Again, the above integral can be asymptotically (for $k_0^{(m)}|x| \gg 1$) put in a more convenient form, by ignoring the rapidly decaying part $|\xi| > k_0^{(m)}$ and using the transformation $\xi = k_0^{(m)} \sin\phi$,

$$\Phi(\boldsymbol{r}, \boldsymbol{r}_0) = Z_0^{(m)}(z) k_0^{(m)} \int_{\phi=-\pi/2}^{\phi=+\pi/2} C_0^{(m)}\left(k_0^{(m)} \sin\phi\right) \times \exp\left(\mathrm{i}k_0^{(m)} \rho \cos(\phi - \psi)\right) \cos(\phi)\, \mathrm{d}\phi, \quad m = 1, 3, \quad \text{(B 2)}$$

where $\rho = \sqrt{x^2 + y^2}$, and $\tan(\psi) = y/|x|$. Under the assumption that the function $C_0^{(m)}(k_0^{(m)} \sin\phi)$ is regular in $-\pi/2 < \phi < \pi/2$ (for which there is evidence that it is valid in the case of monotonic depth functions $h(x), a < x < b$), and applying the method of stationary phase to evaluate the above integral, we obtain at the leading order $O(\rho^{-1/2})$ of approximation,

$$\Phi(\boldsymbol{r}, \boldsymbol{r}_0) \approx \frac{\exp\left(\mathrm{i}k_0^{(m)} \rho\right)}{\sqrt{\rho}} Z_0^{(m)}(z) F\left(\theta; k_0^{(m)}\right), \quad \boldsymbol{r} \in D^{(m)}, \quad m = 1, 3, \quad \text{(B 3}a\text{)}$$

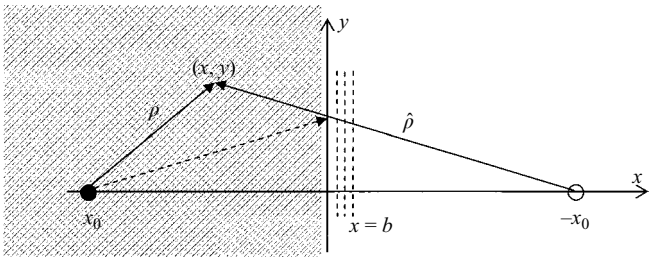

FIGURE 12. Geometrical interpretation of the asymptotic result (B 5). The point source is denoted by a solid circle and its image by an open circle. The region of depth variation is shown by using dashed lines to indicate the parallel bottom contours.

where the far-field pattern $F_m(\theta; k_0^{(m)})$ is given by

$$F_m\big(\theta; k_0^{(m)}\big) = \sqrt{\frac{2\pi}{k_0^{(m)}}}\exp\left(-\frac{\mathrm{i}\pi}{4}\right)k_0^{(m)}|\cos(\theta)|C_0^{(m)}\big(k_0^{(m)}\sin\theta\big), \quad m=1,3, \tag{B 3b}$$

and θ denotes here the field-point angle, $\tan(\theta) = y/x \approx (y-y_0)/(x-x_0)$ (the last approximation being valid for (x, y) lying in the far field, outside $D^{(2)}$. We also see from the above equation that, as $\theta \to \pm\frac{1}{2}\pi \pm 0$, the far-field point $\boldsymbol{r}$ sharply passes from $D^{(m)}$, $m=1, 3$, to $D^{(2)}$ and the far-field pattern $F_m \to 0$. In this case, the asymptotic structure of the wave field is described by the next order of approximation, which is $O(\rho^{-3/2})$. Equations (B 3) are in agreement with the corresponding leading-order asymptotic result for the Green function of the mild-slope equation, Belibassakis (2000, equation (5.11*a*)).

B.2. *The point source in $D^{(m)}$, $m=1$ or 3, far from the bottom irregularity*

In the case where the point source lies in $D^{(m)}$, $m=1$ or 3, at a great distance from $D^{(2)}$, we can derive its leading-order far-field asymptotic structure using the results of Appendix A. Without loss of generality, we shall assume that the source lies in the left-hand half-strip, $\boldsymbol{x}_0 \in D^{(1)}$, $x_0 \ll a$, and we shall set $a=0$. In this case, the transfer function $\mathscr{H}(\boldsymbol{r};\theta)$ simplifies to

$$\mathscr{H}(\boldsymbol{r};\theta) = \big(\exp\big(\mathrm{i}k_0^{(1)}x\cos\theta\big) + A_R(\theta)\exp\big(-\mathrm{i}k_0^{(1)}x\cos\theta\big)\big) \times \exp\big(\mathrm{i}k_0^{(1)}y\sin\theta\big)\cosh\big(k_0^{(1)}(z+h_1)\big), \quad x \ll a, \tag{B 4a}$$

and

$$\mathscr{H}(\boldsymbol{r};\theta) = A_T(\theta)\exp\big(\mathrm{i}k_0^{(3)}(x\cos\theta_3 + y\sin\theta_3)\big)\cosh\big(k_0^{(3)}(z+h_3)\big), \quad x \gg b, \tag{B 4b}$$

where A_R, A_T denote the reflection and transmission coefficients, respectively, and $\theta_3 = \sin^{-1}(k_0^{(1)}\sin\theta/k_0^{(3)})$ is the grazing angle of the wave in $D^{(3)}$. Using the above expressions in (A 6) and applying the method of stationary phase to evaluate the integral, we obtain at the leading order $O(\rho^{-1/2})$ of approximation

$$\Phi_{sng}(\boldsymbol{r}, \boldsymbol{r}_0) \approx A_{sng}\sqrt{\frac{2\pi}{k_0^{(1)}}}\left(\frac{\exp\big(\mathrm{i}k_0^{(1)}\rho - \frac{1}{4}\mathrm{i}\pi\big)}{\sqrt{\rho}} + A_R(\hat{\theta})\frac{\exp\big(\mathrm{i}k_0^{(1)}\hat{\rho} + \frac{1}{4}\mathrm{i}\pi\big)}{\sqrt{\hat{\rho}}}\right)\cosh\big(k_0^{(1)}(z+h_1)\big), \tag{B 5}$$

for $x \ll a$, where $\tan(\hat{\theta}) = y/|x+x_0|$, and $\hat{\rho} = \sqrt{(x+x_0)^2+y^2}$. The geometrical interpretation of the above result is shown in figure 12. The above result is similar

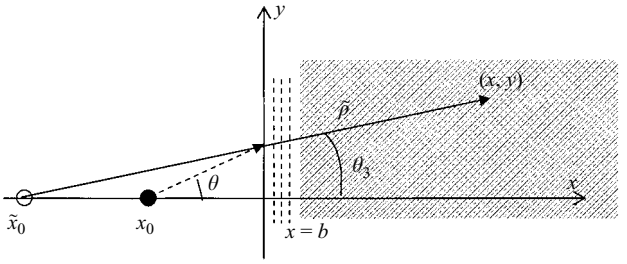

FIGURE 13. Geometrical interpretation of the asymptotic result (B 7), in the case $k_0^{(3)} > k_0^{(1)}$. The point source is denoted by a solid circle. The region of validity of this result is shown as a shaded area.

to the leading asymptotic expansion of the wave field of a point two-dimensional time-harmonic acoustic source in a plane discontinuous medium; see e.g, Felsen & Marcuvitz (1973, § 5.5e).

An analogous result can be obtained for $x \gg b > a$, in the case $y/(x-x_0) \ll 1$ (which, since we have assumed $\boldsymbol{x}_0 \in D^{(1)}$, $x_0 \ll a$, becomes the most important case from the point of view of applications), by using the small-angle approximation ($\theta_3 \approx \theta k_0^{(1)}/k_0^{(3)}$). This assumption permits us to express the phase of the integrand on the right-hand side of (A 6) as follows:

$$S(\theta) = k_0^{(3)}(x\cos\theta_3 + y\sin\theta_3) - k_0^{(1)}x_0 \approx k_0^{(3)}\tilde{\rho}\cos\left(\frac{k_0^{(1)}}{k_0^{(3)}}\theta - \psi\right), \tag{B 6}$$

where $\tan(\psi) = y/|x-\tilde{x}_0|$, $\tilde{\rho} = \sqrt{(x-\tilde{x}_0)^2 + y^2}$ and $\tilde{x}_0 = x_0 k_0^{(1)}/k_0^{(3)}$. Applying again the method of stationary phase to evaluate the integral (A 6), we obtain at the leading order $O(\rho^{-1/2})$ of approximation

$$\Phi_{sng}(\boldsymbol{r}, \boldsymbol{r}_0) \approx A_{sng}A_T\left(\psi k_0^{(3)}/k_0^{(1)}\right)\sqrt{\frac{2\pi}{k_0^{(3)}}}\frac{\exp\left(\mathrm{i}k_0^{(3)}\tilde{\rho} - \frac{1}{4}\mathrm{i}\pi\right)}{\sqrt{\tilde{\rho}}}\cosh\left(k_0^{(3)}(z+h_3)\right), \quad x \gg b. \tag{B 7}$$

The geometrical interpretation of the above result, in the case $k_0^{(3)} > k_0^{(1)}$, is shown in figure 13.

REFERENCES

ATHANASSOULIS, G. A. & BELIBASSAKIS, K. A. 1997 Water wave Green's function for a 3D uneven bottom problem with different depths at $x \to +\infty$ and $x \to -\infty$. *Proc. IUTAM Symposium on Computational Methods for Unbounded Domains, July 27–31, 1997, University of Colorado at Boulder*.

ATHANASSOULIS, G. A. & BELIBASSAKIS, K. A. 1999 A consistent coupled-mode theory for the propagation of small-amplitude water waves over variable bathymetry regions. *J. Fluid Mech.* **389**, 275–301.

ATHANASSOULIS, G. A. & BELIBASSAKIS, K. A. 2003 Rapidly-convergent local-mode representations for wave propagation and scattering in curved-boundary waveguides. *6th Intl Conf. on Mathematical and Numerical Aspects of Wave Propagation (WAVES 2003), Finland* (ed. G. Cohen, E. Heikkola, P. Joly & P. Neittaanmäki), Springer.

BAI, K. J. & YEUNG, R. W. 1974 Numerical Solution to free-surface flow problems. *Proc. 10th Naval Hydrodynamics Symposium, Office of Naval Research, Cambridge, MA*, pp. 609–641.

BELIBASSAKIS, K. A. 2000 The Green's function of the mild-slope equation. The case of a monotonic bed profile. *Wave Motion* **32**, 339–361.

Belibassakis, K. A. 2004 Wave–body–seabed interaction in variable bathymetry regions; frequency-domain analysis. (In preparation).

Belibassakis, K. A., Athanassoulis, G. A. & Gerosthathis, T. P. 2001 A coupled-mode model for the refraction-diffraction of linear waves over steep three-dimensional bathymetry. *Appl. Ocean Res.* **23**, 319–336.

Bender, C. M. & Orszag, S. A. 1978 *Advanced Mathematical Methods for Scientists and Engineers.* Mc Graw-Hill.

Brekhovskikh, L. M. & Godin, O. A. 1992 *Acoustics of Layered Media II. Point Sources and Bounded Beams.* Springer.

Coddington, E. A. & Levinson, N. 1955 *Theory of Ordinary Differential Equations.* McGraw Hill.

Di Napoli, F. R. & Deavenport, R. L. 1980 Theoretical and numerical Green's function solution in a plane layered medium. *J. Acoust. Soc. Am.* **67**, 92–105.

Elliot, D. F. & RAO, H. 1982 *Fast Transforms: Algorithms, Analyses, Applications.* Academic.

Euvrard, D., Jami, A., Lenoir, M. & Martin, D. 1981 Recent progress towards an optimal couping between finite elements and singularity distribution procedures, *Proc. 3rd Intl Conf. on Numerical Ship Hydrodynamics*, pp. 193–210.

Evans, D. V. 1972 The application of a new source potential to the problem of the transmission of water waves over a shelf of arbitrary profile. *Proc. Camb. Phil. Soc.* **71**, 391–410.

Felsen, L. B. & Marcuvitz, N. 1973 *Radiation and Scattering of Waves.* Prentice Hall.

Frisk, G. V. 1994 *Ocean and Seabed Acoustics.* Prentice Hall.

Geckinkli, N. C. & Yavuz, D. 1983 *Discrete Fourier Transformation and its Applications to Power Spectra Estimation.* Elsevier.

Gohberg, I. C. & Krein, M. G. 1969 *Introduction to the Theory of Linear Nonselfadjoint Operators.* American Mathematical Society.

Gradshteyn, I. S. & Ryzhik, I. M. 1965 *Tables of Integrals Series and Products.* Academic.

Guo, Y. P. 1987 Waves induced by sources near the ocean surface. *J. Fluid Mech.* **181**, 293–310.

Jensen, F. B., Kuperman, W. A., Porter, M. B. & Schmidt, H. 1984 *Computational Ocean Acoustics.* AIP Press.

John, F. 1950 On the motion of floating bodies. *Comm. Pure Appl. Maths* **3**, 45–101.

Markushevich, A. I. 1965 *Theory of Functions of a Complex Variable.* Chelsea Publishing Company, New York.

Mei, C. C. 1983 *The Applied Dynamics of Ocean Surface Waves.* John Wiley & Sons (2nd Reprint, 1994, World Scientific).

Miles, J. W. 1967 Surface-wave scattering matrix for a shelf. *J. Fluid Mech.* **28**, 755–767.

Newman, J. N. 1985 Algorithms for the free-surface Green function. *J. Engng Maths* **19**, 57–67.

Noble, B. 1958 *Methods based on the Wiener-Hopf technique.* Chelsea Publishing Company, New York.

Oden, J. T. & Reddy, J. N. 1976 *An Introduction to the Mathematical Theory of Finite Elements.* John Wiley & Sons.

Oppenheim, A. V. & Schafer, R. W. 1989 *Disrete-Time Signal-Processing.* Prentice Hall.

Sidorov, Y. V., Fedoryuk, M. V. & Shabunin, M. I. 1985 *Lectures on the Theory of Complex Functions.* MIR Publishers, Moscow.

Stoker, J. J. 1957 *Water Waves.* Interscience.

Thorne, R. C. 1953 Multipole expansions in the theory of surface waves. *Proc. Camb. Phi. Soc.* **49**, 707–716.

Vainberg, B. R. & Maz'ja, V. G. 1973 On the problem of steady state oscillations of a fluid layer of variable depth. *Trans. Moscow Math. Soc.* **28**, 56–73.

Vladimirov, V. S. 1984 *Equations of Mathematical Physics.* MIR Publishers, Moscow.

Wehausen, J. N. 1974 Methods for boundary-value problems in free-surface flows. *David Taylor Naval Ship Res. and Development Center, DTNSRDC Rep.* 4622, Bethesda MD.

Wehausen, J. N. & Laitone, E. V. 1960 *Surface Waves.* Handbuch der Physik. Springer.